The Astrophysical Journal, 692:618–652, 2009 February 10 doi:10.1088/0004-637X/692/1/618

THE PHYSICAL PROPERTIES AND EFFECTIVE TEMPERATURE SCALE OF O-TYPE STARS AS A FUNCTION OF METALLICITY. III. MORE RESULTS FROM THE MAGELLANIC CLOUDS*

Philip Massey[1], Amanda M. Zangari[1,6], Nidia I. Morrell[2], Joachim Puls[3], Kathleen DeGioia-Eastwood[4], Fabio Bresolin[5], and Rolf-Peter Kudritzki[5]
[1] Lowell Observatory, 1400 W Mars Hill Road, Flagstaff, AZ 86001, USA; phil.massey@lowell.edu, azangari@mit.edu
[2] Las Campanas Observatory, The Carnegie Observatories, Colina El Pino s/n, Casilla 601, La Serena, Chile; nmorrell@lco.cl
[3] Universitäts-Sternwarte München, Scheinerstr. 1, 81679 München, Germany; uh101aw@usm.uni-muenchen.de
[4] Department of Physics and Astronomy, Northern Arizona University, P.O. Box 6010, Flagstaff, AZ 86011-6010, USA; kathy.eastwood@nau.edu
[5] Institute for Astronomy, 2680 Woodlawn Drive, Honolulu, HI 26822-1839, USA; bresolin@ifa.hawaii.edu, kud@ifa.hawaii.edu
Received 2008 July 29; accepted 2008 October 21; published 2009 February 19

ABSTRACT

In order to better determine the physical properties of hot, massive stars as a function of metallicity, we obtained very high signal-to-noise ratio optical spectra of 26 O and early B stars in the Magellanic Clouds. These allow accurate modeling even in cases where the He I λ4471 line has an equivalent width of only a few tens of m Å. The spectra were modeled with FASTWIND, with good fits obtained for 18 stars; the remainder show signatures of being binaries. We include stars in common to recent studies to investigate possible systematic differences. The "automatic" FASTWIND modeling method of Mokiem and collaborators produced temperatures 1100 K hotter on average, presumably due to the different emphasis given to various temperature-sensitive lines. More significant, however, is that the automatic method always produced a "best" result for each star, even ones we identify as composite (binaries). The temperatures found by the TLUSTY/CMFGEN modeling of Bouret, Heap, and collaborators yielded temperatures 1000 K cooler than ours, on average. Significant outliers were due either to real differences in the data (some of the Bouret/Heap data were contaminated by moonlight continua) or the fact that we could detect the He I line needed to better constrain the temperature. Our new data agree well with the effective temperature scale we previously presented. We confirm that the "Of" emission characteristics do not track luminosity classes in exactly the same manner as in Milky Way stars. We revisit the issue of the "mass discrepancy," finding that some of the stars in our sample do have spectroscopic masses that are significantly smaller than those derived from stellar evolutionary models. We do not find that the size of the mass discrepancy is simply related to either effective temperature or surface gravity.

Key words: stars: atmospheres – stars: early-type – stars: fundamental parameters – stars: mass loss

Online-only material: color figures

1. INTRODUCTION

The highest-mass stars spend their main-sequence lifetimes as O-type dwarfs, giants, and supergiants, and as early B-type giants and supergiants.[7] In order to determine their physical properties (effective temperatures, bolometric luminosities, stellar radii, surface gravities, etc.), we must rely upon modeling their spectra, as these stars are so hot that their optical and UV colors have only slight dependence on their physical properties, even effective temperature (see Massey 1998a, 1998b).

The stellar atmospheres of such stars are physically complex, and producing realistic synthetic spectra requires the inclusion of non-LTE (NLTE), as well as careful treatment of the hydrodynamics of the stellar wind. The recent inclusion of line blanketing in these models has led to a significant lowering of the effective temperature scale for Galactic O-type stars (Martins et al. 2002; Bianchi & Garcia 2002; Repolust et al. 2004; Martins et al. 2005). Such a change has a strong effect on the expected amount of ionizing radiation for stars of a given spectral type; it also has (as yet largely unconsidered) implications for the previous determinations of the ages of young Galactic clusters and OB associations, and stellar evolutionary theory, as the theoretical zero-age main sequence (ZAMS) may now be too hot for the locations of stars in the Hertzsprung-Russell (H–R) diagram.

In two previous papers (Massey et al. 2004, 2005; hereafter, Papers I and II, respectively), we used *Hubble Space Telescope* (*HST*) and ground-based optical and UV data to determine the effective temperatures of O stars in the Large Magellanic Cloud (LMC) and Small Magellanic Cloud (SMC). Many O stars of the earliest type (O2–O4) were included in this sample. Our expectations were that since the metallicity is lower in the SMC and LMC ($Z/Z_\odot = 0.2$ and $Z/Z_\odot = 0.5$; Russell & Dopita 1990 and discussion in Paper I) than in the Milky Way, the effects of stellar wind blanketing and line blanketing would be less, with the result that the effective temperatures of O stars would be hotter in the Clouds than in their Galactic counterparts. Indeed, this was what we found: SMC stars of spectral type O3–7 V were found to be 4000 K hotter than Galactic stars of the same spectral type, with stars of a slightly later type showing

* This paper is based on data gathered with the 6.5 m Magellan telescopes located at Las Campanas Observatory, Chile, and also on observations made with the NASA/ESA *Hubble Space Telescope,* obtained from the Data Archive at the Space Telescope Science Institute (STScI), which is operated by the Association of Universities for Research in Astronomy, Inc., under NASA contract NAS 5-26555. These observations are associated with programs 9412, 9795, and 11270.

[6] Astronomy Department, Wellesley College, Wellesley, MA 024871. Research Experiences for Undergraduates (REU) participant, Summer 2007. Current address: Department of Earth, Atmospheric, and Planetary Sciences, Massachusetts Institute of Technology, Cambridge, MA 02139, USA.

[7] Unlike the case for stars of lower mass, "dwarf" and "main sequence" are not synonymous terms, as high-mass stars will become O and B supergiants while still on the hydrogen-burning main sequence.

increasingly smaller effects until B0 V, at which type there was no discernible effect. The supergiants show a similar effect. The effective temperatures of LMC O stars, for which the metallicity is intermediate between that of the SMC and the Milky Way, are between that of the SMC and the Milky Way. In contrast, Heap et al. (2006) found relatively low effective temperatures for a sample of SMC O stars. (Their study included their earlier work, presented in Bouret et al. 2003.) In Paper II, we argued that this may have been due to a lack of nebular subtraction in their short-slit Echelle data, particularly for stars in NGC 346, one of the strongest H II regions in the SMC, and/or a consequence of the "sky-subtraction" method used for their data as described by Walborn et al. (2000), which would result in incorrect continuum levels being assigned.

A necessary input in such modeling efforts is the terminal velocity of the stellar wind, which we primarily measure from the C IV λ1550 doublet. By the time we finished Papers I and II, the astronomical community had lost its only resource for such work, the Space Telescope Imaging Spectrograph (STIS) on *HST*, and it appeared that it would be many years before such data could be again obtained.[8] However, we found that there were a significant number of Magellanic Cloud O-type stars observed with STIS UV data available in the archives, but which had not been included in Paper I or II.

We therefore decided to obtain very high signal-to-noise ratio (S/N) optical data on this remaining subset of stars and to determine the physical properties of these stars via modeling with FASTWIND (Santolaya-Rey et al. 1997; Puls et al. 2005), performing an analysis similar to that of Papers I and II. The sample included not only some of the NGC 346 stars analyzed by Bouret et al. (2003) and Heap et al. (2006), allowing us to resolve that controversy, but also stars of spectral subtypes poorly represented in Papers I and II. Our analysis here will follow closely that of Papers I and II. We use archival STIS UV spectra to determine the star's terminal velocity v_∞. In order to provide a consistency check, we also decided to re-observe two of the stars analyzed in Papers I and II in order to see how reproducible our answers are given slight differences in instrumentation, rectification, etc. We describe our data and reduction procedures in Section 2. We present our analysis in Section 3. In Section 4, we give our results, compare our work with those of others, and incorporate the new sample into our effective temperature scales.

2. OBSERVATIONS AND REDUCTIONS

In Table 1, we list the 26 stars selected for study. These stars were primarily chosen because they were of O-type and (nominally) had UV spectra in the *HST* archives.We included some stars from previous studies, including two stars from our own work as a consistency check. Not all stars were successfully modeled, for reasons we will describe below.

The spectra used in this study were obtained by P.M., N.I.M., and K.D.E. on UT 2004 November 27–29 using the Boller & Chivens Spectrograph on the Clay 6.5 m (Magellan II) telescope on Las Campanas. The instrument uses a 2048 × 515 Marconi CCD with 13.5 μm pixels. On the first two nights, observations were made in the blue, with a 1200 line mm^{-1} grating blazed at 4000 Å. The wavelength coverage extended from 3410 to 5040 Å. We used a 1″ slit (350 μm) to achieve a spectral resolution of 2.4 Å (3.0 pixels). The resolution degraded significantly shortward of 3500 Å, and we do not use those data. On the third night, observations were made in the red, with a 1200 line mm^{-1} grating blazed at 7500 Å. The wavelength coverage was 5315–6950 Å, with similar resolution. No blocking filter was used with either grating.

For the blue exposures, which include most of the weak absorption lines we used in our modeling, we took a series of three consecutive exposures for each target, aiming for a total S/N of 600 per spectral resolution element at 4500 Å (i.e., each of the three exposures had a S/N of 350.) To achieve this, we adjusted our exposure times so that we observed a $B = 13.0$ mag star for a total of 600 s (i.e., 3 × 200 s exposures). For the red, we were satisfied with a slightly lower S/N (since we were primarily interested in Hα) and aimed for a total S/N of 400 per spectral resolution element at 6500 Å, which we achieved in 3 × 200 s at $V = 13.0$ mag. Each observation was obtained at the parallactic angle, as the instrument was used without an atmospheric dispersion corrector.

The CCD data were reduced using IRAF.[9] The images were trimmed and a bias level subtracted using the overscan. Nine bias exposures (0 s exposures) were averaged and were used to remove any residual two-dimensional structure, although none was evident in our examination of the images. Nine flat-field exposures were obtained each night using the projector flat, with a count level below saturation but whose total number of counts was such that the S/N of our program data was not degraded. Twilight sky exposures were used to correct for the slight difference in the illumination function along the slit between the program data and the dome flats. A series of long and short flat-field exposures were used to construct a bad pixel map for the CCD, and the data linearly interpolated over bad columns.

Next, the stellar spectra were extracted (following Massey et al. 1992) using variance weighting across the spatial direction. The "clean" function was used in order to recognize and remove cosmic rays at this point. A series of long comparison (HeNeAr) arc exposures obtained at the beginning of the night was used for the wavelength correction; tests showed that there was very little flexure within the instrument throughout the night as the instrument rotated about the optical axis at the Nasmyth focus.

Getting the rectification (normalization) "right" is important for O stars, particularly for weak lines and for the wings of the Balmer lines. Each individual spectrum was normalized before combining, with the blue data first clipped below 3800 Å to remove the effect of the Balmer jump on the normalization. The normalization was done interactively using a seventh-order cubic spline, with care taken to examine the regions around the principle classification/modeling lines. The three normalized spectra obtained in each wavelength region for each star were then averaged using an algorithm that rejected deviant pixels.

3. ANALYSIS

3.1. Spectral Classification

We began by first classifying the stars as to spectral type and luminosity class. The spectral types were qualitatively determined by comparing the spectra with standards from

[8] The resurrection of STIS is included on the agenda for Servicing Mission 4, currently due to be launched in 2009 May.

[9] IRAF is distributed by the National Optical Astronomy Observatory, which is operated by the Association of Universities for Research in Astronomy, Inc., under cooperative agreement with the National Science Foundation (NSF). We are grateful to the ongoing support of IRAF and the help "desk" maintained by the volunteers at http://www.iraf.net.

Table 1
Sample of Stars

Star[a]	Type[b]	Galaxy	α_{2000}	δ_{2000}	V	$U-B$	$B-V$	$A_V(B-V)$[c]	$A_V(U-B)$[c]	M_V[d]	Comments
AzV 15	O6.5 I(f)	SMC	00 46 42.17	−73 24 55.2	13.12	−1.03	−0.19	0.37	0.56	−6.15	···
AzV 61	O5.5 III((f))	SMC	00 50 01.77	−72 11 26.0	13.54	−1.05	−0.18	0.43	0.60	−5.79	···
AzV 75	O5.5 I(f)	SMC	00 50 32.39	−72 52 36.1	12.70	−1.00	−0.15	0.50	0.73	−6.70	···
AzV 83	O7 Iaf	SMC	00 50 52.05	−72 42 14.8	13.31	−0.96	−0.12	0.59	0.78	−6.18	···
NGC 346−324	O5 V	SMC	00 58 57.38[e]	−72 10 33.7[e]	14.02[f]	−1.05[f]	−0.24[f]	0.25	0.60	−5.13	NGC 346 W6
NGC 346−342	O5.5 III((f))	SMC	00 59 00.04[e]	−72 10 37.9[e]	13.66[f]	−1.05[f]	−0.23[f]	0.28	0.52	−5.52	NGC 346 W4
NGC 346−355	O2 V	SMC	00 59 00.75[e]	−72 10 28.2[e]	13.50[f]	−1.12[f]	−0.23[f]	0.31	0.34	−5.71	NGC 346 W3
NGC 346−368	O6 V	SMC	00 59 01.81[e]	−72 10 31.3[e]	14.18[f]	−1.08[f]	−0.23[f]	0.28	0.43	−5.00	···
NGC 346−487	O8 V	SMC	00 59 06.71[e]	−72 10 41.3[e]	14.53[f]	−1.01[f]	−0.22[f]	0.28	0.56	−4.65	···
AzV 223	O9.5 II	SMC	00 59 13.41	−72 39 02.2	13.66	−0.98	−0.14	0.40	0.43	−5.64	···
NGC 346−682	O8 V	SMC	00 59 18.63[e]	−72 11 10.0[e]	14.87[f]	−1.02[f]	−0.24[f]	0.22	0.52	−4.25	···
AzV 232	O7 Iaf+	SMC	00 59 31.97[e]	−72 10 46.1[e]	12.31[f]	−1.05[f]	−0.19[f]	0.37	0.39	−6.96	Sk 80, NGC346−789
AzV 327	O9.7 I	SMC	01 03 10.49	−72 02 14.2	13.03	−1.04	−0.16	0.37	0.43	−6.24	···
AzV 388	O5.5 V((f))	SMC	01 05 39.45	−72 29 26.8	14.09	−1.07	−0.21	0.34	0.52	−5.15	···
BI 9	O7.5 III((f))	LMC	04 52 47.95	−68 47 39.1	13.70	−0.99	−0.22	0.31	0.65	−5.11	···
LMC 054383	O4-5 V((f))pec	LMC	05 02 09.94	−70 32 58.1	14.10	−1.08	−0.19	0.43	0.52	−4.83	···
Sk −70 60	O4-5 V((f))pec	LMC	05 04 40.88	−70 15 34.7	13.88	−1.09	−0.16	0.53	0.47	−5.15	···
Sk −70 69	O5.5 V((f))	LMC	05 05 18.69	−70 25 50.3	13.95	−1.09	−0.23	0.28	0.43	−4.83	···
Sk −68 41	B0.5 Ia	LMC	05 05 27.20[e]	−68 10 02.8[e]	12.04[g]	−0.93[g]	−0.14[g]	0.25	0.47	−6.71	···
Sk −69 124	O9.7 I	LMC	05 25 18.35	−69 03 11.3	12.77	−1.03	−0.16	0.34	0.21	−6.07	···
BI 170	O9.5 I	LMC	05 26 47.79	−69 06 11.9	13.06	−1.04	−0.20	0.22	0.17	−5.66	···
BI 173	08.5 II(f)	LMC	05 27 10.05	−69 07 56.3	12.96	−1.02	−0.16	0.39	0.52	−5.93	···
LH 64−16	ON2 III(f*)	LMC	05 28 46.97	−68 47 47.9	13.61	−1.11	−0.22	0.34	0.39	−5.23	···
Sk −67 166	O4 If	LMC	05 31 44.30	−67 38 01.0	12.27[g]	−1.01[g]	−0.22[g]	0.31	0.73	−6.54	HD 269698
BI 192	O9 III	LMC	05 32 00.00	−67 32 55.4	13.75	−1.03	−0.22	0.28	0.43	−5.03	···
BI 208	O6 V((f))	LMC	05 33 57.38	−67 24 20.3	13.94	−1.09	−0.22	0.31	0.39	−4.87	···

Notes. Units of right ascension are hours, minutes, and seconds, and units of declination are degrees, arcminutes, and arcseconds. Coordinates and photometry from Massey (2002) unless otherwise noted.

[a] Star names are from the following catalogs: "AzV" from Azzopardi & Vigneuau (1975); "NGC 346" from Massey et al. 1989, and known to CDS as Cl* "NGC 346 MPG;" "Sk," from Sanduleak (1970); "BI" from Brunet et al. (1975); "LMC" from Massey 2002, and known to CDS as [M2002]; "LH 64−16," from Lucke (1973); see also Massey et al. (2000).

[b] From this paper.

[c] $A_V(B-V) = 3.1[(B-V)-(B-V)_0]$ and $A_V(U-B) = 4.3[(U-B)-(U-B)_0]$, where $(B-V)_0$ and $(U-B)_0$ are the intrinsic colors for stars of a given spectral type, taken from Massey (1998b).

[d] Based upon $V - 3.1E(B-V)$−DM, where the DM is assumed to be 18.9 for the SMC and 18.5 for the LMC.

[e] Coordinates newly determined in this paper.

[f] Stars in NGC 346 have photometry from Massey et al. (1989).

[g] Photometry taken from Buscombe & Foster (1995).

Walborn & Fitzpatrick (1990). A quantitative determination of the types was also obtained by measuring the equivalent widths (EWs) (by direct integration) of He I λ4471 and He II λ4542, and calculating $\log W' = \log \frac{W(\mathrm{He\,I}\,\lambda4471)}{W(\mathrm{He\,II}\,\lambda4542)}$. This $\log W'$ value was compared against the calibration of Conti (1988).

As we discussed in Paper I, we expect our ability to detect and measure faint lines to be limited by our spectral resolution r and the S/N: $\sigma_{\mathrm{EW}} = r/(\mathrm{S/N})$. For r =2.4 Å, and a S/N of 600, we expect the uncertainty to be about 4 m Å. Thus, we should be able to detect lines at the 3σ level of 12 m Å. In practice, our measurement of the EWs (which we use only as a second check on the spectral classification) is limited more by the exact rectification, and is typically 20 m Å, although in some cases it is better than this.

For Milky Way stars, the luminosity class is primarily determined by the "f" characteristics in the spectra: a luminosity class "V" star (dwarf) will have N III λλ4634, 42 in weak emission, but He II λ4686 in strong absorption, designated by the spectroscopic notation "((f))." A luminosity class "III" star (giant) will have the N III lines in somewhat stronger emission and the He II λ4686 line partially filled in by emission, denoted by the spectroscopic notation "(f)." A luminosity class "I" star (supergiant) will have both the N III λλ4634, 42 lines and He II λ4686 line in strong emission, denoted by the spectroscopic notation "f." Thus, these classes would be designated somewhat redundantly as "V((f))," "III(f)," and "If." The situation is a little more complicated than that for the later O stars, as the "((f))" characteristic does not manifest itself until luminosity class III, and by O9 none of these are found in emission and instead one uses the relative strengths of Si IV λλ4116 to He I λ4121 to assign luminosity classes.

The difficulty with extending this to lower metallicity is as follows. As first noted by Mihalas et al. (1972), the N III λλ4634, 42 lines go into emission as a result of dielectric recombination, while the He II λ4686 emission is formed in the stellar wind. Thus, at lower metallicity, we might expect that the N III λλ4634, 42 emission formation will take place at about the same physical conditions, but that the He II λ4686 emission will not—at a given effective temperature, a higher luminosity will be needed for the same stellar wind strength and He II λ4686 emission. Thus, in the SMC, on simple theoretical grounds, it is *expected* to have "I(f)" supergiants while in the Milky Way stars with the same basic properties (effective temperatures, surface

gravity, and luminosity) would result in a spectral appearance of "If." This was certainly what we found in Papers I and II. Additionally, subtle luminosity/spectral-type criteria, such as the presence of Si IV λλ4089, 16 (denoted by some by the notation "f+"), go into emission due to selective emission mechanisms, and their behavior may also differ with the spectral type from what we are used to from Milky Way examples. Therefore, in assigning luminosity classes, we first classified the star as if it were a Galactic star, but then paid attention to any large difference between the absolute visual magnitude we derived and the absolute visual magnitude we expected for the spectral type and luminosity class. Of course, if the visual luminosity was greater than what we expect, this could also be an indication of binarity, and we carefully examined our spectra for telltale signs, such as the inability to obtain good fits of both the He I and He II lines with a single set of parameters. The classification of each star is given in Table 1 and will be individually discussed in Section 3.4. When all is said and done, we expect that our spectral types are good to one classification step, that is, an O8 V star could be reasonably classified as O7.5 V or O8.5 V.

3.2. Input: M_V and v_∞

In order to model the spectra of the stars with FASTWIND, we need two additional constraints. The first of these is the absolute visual magnitude M_V, which is needed to calculate the stellar radius for a given set of inputs, and is found from existing photometry and knowledge of the intrinsic colors, which in turn comes from the spectral type. The second of these is the terminal velocity of the wind v_∞, which we can best measure by using the resonance lines in the UV part of the spectra.

In order to derive an accurate M_V, we began by adopting the intrinsic colors corresponding to the spectral types, using Table 3 of Massey (1998b). We then calculated M_V from

$$M_V = V - 3.1E(B-V) + \mathrm{DM},$$

where the distance modulus (DM) is assumed to be 18.9 for the SMC and 18.5 for the LMC, following van den Bergh (2000). This value was compared with that expected for the assigned luminosity class (Conti et al. 1983). If there was a significant discrepancy, we reassigned a more appropriate luminosity class as discussed above. We then recalculated the final M_V using the more appropriate intrinsic color. (In practice, this made very little difference, as the differences in intrinsic colors of O-type stars change by 0.03 mag in $B-V$ as a function of the luminosity class.) The adopted A_V and M_V values are included in Table 1. We also include the A_V determined from the $U-B$ colors as a reality check on the A_V values determined from $E(B-V)$. In general, the agreement is good, with an average difference of $A_V(U-B) - A_V(B-V) = 0.15$ and a scatter of 0.13. We adopt the A_V determined from $E(B-V)$ as the $B-V$ values are generally more accurately determined than $U-B$. The slight systematic offset may also represent how poorly we still know the intrinsic colors of O stars at differing metallicities (see, e.g., the nice work by Martins & Plez 2006).

The other ingredient for modeling the optical spectra is knowledge of the terminal velocity (v_∞) of the wind. Many of our stars had well measured values in the literature, while for others we measured these ourselves using the methods described in Paper I. For one of the stars, LMC 054383, we obtained new UV data. We list the measured values and sources in Table 2. Two stars require additional comments. At the time we planned our Magellan observations, we thought that NGC 346−682 had a STIS spectrum, but Heap et al. (2006) noted that the acquisition had failed. A second star, NGC 346−487, has only a lower limit on the terminal velocity. We have decided to retain both of these stars in our analysis anyway and, following Kudritzki & Puls (2000), we adopt a value of $v_\infty = 2.6v_{\rm esc}$, where the *effective* escape velocity $v_{\rm esc}$ is calculated from the stellar radius R and surface gravity g, explictly including the Eddington factor Γ, that is,

Table 2
Adopted Terminal Velocities v_∞

Star	Type	Galaxy	v_∞ (km s^{-1})	Ref.	$2.6v_{\rm esc}$ (km s^{-1})
AzV 15	O6.5 I(f)	SMC	2125	1	2100
AzV 61	O5.5 III((f))	SMC	2025	1	···
AzV 75	O5.5 I(f)	SMC	2120	2	1860
AzV 83	O7 Iaf	SMC	930	1	···
NGC 346−324	O5 V	SMC	2300	3	2450
NGC 346−342	O5.5 III((f))	SMC	1945	4	···
NGC 346−355	O2 V	SMC	2800	3	2200
NGC 346−368	O6 V	SMC	2100	3	···
NGC 346−487	O8 V	SMC	$\geqslant$1100	3	3500[a]
AzV 223	O9.5 II	SMC	1680	5	1950
NGC 346−682	O8 V	SMC	···	5	2900
AzV 232	O7 Iaf+	SMC	1400	6	···
AzV 327	O9.7 I	SMC	1500	1	1460
AzV 388	O5.5 V((f))	SMC	1935	4	2440
BI 9	O7.5 III((f))	LMC	1900	4	···
LMC 054383	O4-5V((f))pec	LMC	2380	5	···
Sk −70 60	O4-5V((f))pec	LMC	2150	4	···
Sk −70 69	O5.5 V((f))	LMC	2300:	4	1720
Sk −68 41	B0.5 Ia	LMC	865	4	1300
Sk −69 124	O9.7 I	LMC	1430	4	1240
BI 170	O9.5 I	LMC	1370	4	1120
BI 173	08.5 II(f)	LMC	1950:	4	1630
LH 64−16	ON2 III(f*)	LMC	3250	5	1475
Sk −67 166	O4 If	LMC	735	4	···
BI 192	O9 III	LMC	1100:	4	1670
BI 208	O6 V((f))	LMC	980:	4	2110

Note. [a] Adopted.
References. (1) Evans et al. (2004); (2) Paper I; (3) Bouret et al. (2003); (4) Prinja & Crowther (1998); (5) This paper; (6) Puls et al. (1996).

$$v_{\rm esc} = \sqrt{1.392 \times 10^{11}(R/R_\odot)\, g(1-\Gamma)},$$

$$\Gamma = 0.4\, N_e\, Y_{\rm He}\, g\left[(1+4Y_{\rm He})\, 1.8913 \times 10^{-15}\, T_{\rm eff}^4\right]^{-1},$$

where N_e is the number of free electrons per He atom (2 for $T_{\rm eff} > 28{,}000$, otherwise 1 for OB stars) and $Y_{\rm He}$ is the number ratio of He to H. The surface gravity g is in cgs units (i.e., for the sun $\log g = 4.438$). We expect that the factor of proportionality of 2.6 will be fairly insensitive to the metallicity, but one needs to keep in mind that this number is good only to 20% and that this scaling relationship is approximate in any event (Kudritzki & Puls 2000), so we have used rounded values for these two stars. Given the spectral types, neither of these stars is expected to have strong winds. For comparison, we include the values of $2.6v_{\rm esc}$, drawing on the results of the model fitting presented below, for the other stars, where we see that in general there was very good agreement.

3.3. Methodology

The spectra were fitted by varying the trial surface gravity, effective temperatures, and mass-loss rates in the models, and

Table 3
Results of Model Fits

Star	Type	Galaxy	v_r km s^{-1}	$v \sin i$ km s^{-1}	$T_{\rm eff}$ (K)	log $g_{\rm eff}$ [cgs]	log $g_{\rm true}$ [cgs]	$R/R_\odot$	M_V (mag)	BC (mag)	log $L/L_\odot$	$m_{\rm spect}$ $M_\odot$	$m_{\rm evol}$[a] $M_\odot$	$\dot{M}$[b]	β	v_∞ km s^{-1}	He/H[c]	Comments
AzV 15	O6.5 I(f)	SMC	130	180	38500	3.6	3.63	18.3	−6.15	−3.66	5.82	52	54	1.8	0.8	2125	0.10	Previously modeled
AzV 61	O5.5 III((f))	SMC	···	···	···	···	···	···	−5.79	···	···	···	···	···	···	2025	···	Disk signature
AzV 75	O5.5 I(f)	SMC	140	180	39500	3.5	3.52	23.4	−6.70	−3.75	6.08	66	78	3.0	0.8	2120	0.10	Previously modeled
AzV 83	O7 Iaf	SMC	···	···	···	···	···	···	−6.18	···	···	···	···	···	···	926	···	Previously modeled but binary?
NGC 346−324	O5 V	SMC	170	150	42000	3.9	3.91	10.8	−5.13	−3.91	5.51	35	41	0.6	0.8	2300	0.10	Previously modeled
NGC 346−342	O5.5 III((f))	SMC	···	···	···	···	···	···	−5.52	···	···	···	···	···	···	1945	···	Ecl. binary
NGC 346−355	O2 V	SMC	190	140	49500	3.9	3.92	12.8	−5.71	−4.42	5.95	50	75	2.0	0.8	2800	0.10	Previously modeled
NGC 346−368	O6 V	SMC	···	···	···	···	···	···	−5.00	···	···	···	···	···	···	2100	···	Previously modeled but binary?
NGC 346−487	O8 V	SMC	170	160	38000	4.2	4.21	9.1	−4.65	−3.58	5.19	49	29	0.1	0.8	3500	0.10	Previously modeled
AzV 223	O9.5 II	SMC	190	140	32000	3.5	3.52	16.4	−5.64	−3.12	5.40	32	32	0.5	0.8	1680	0.10	
NGC 346−682	O8 V	SMC	180	150	36000	4.1	4.11	7.8	−4.25	−3.41	4.97	33	23	0.05	0.8	2900	0.10	Previously modeled
AzV 232	O7 Iaf+	SMC	···	···	···	···	···	···	−6.96	···	···	···	···	···	···	1400	···	Previously modeled but binary?
AzV 327	O9.7 I	SMC	190	150	30800	3.2	3.23	22.1	−6.24	−3.01	5.60	30	37	0.7	0.8	1500	0.15	Previously modeled
AzV 388	O5.5 V((f))	SMC	190	190	42500	3.9	3.92	10.8	−5.15	−3.94	5.53	35	42	0.3	0.8	1935	0.10	Previously modeled
BI 9	O7.5 III((f))	LMC	···	···	···	···	···	···	−5.46	···	···	···	···	···	···	1900	···	No good fit–binary?
LMC 054383	O4-5V((f))pec	LMC	···	···	···	···	···	···	−4.83	···	···	···	···	···	···	2380	···	Disk signature
Sk −70 60	O4-5 V((f))pec	LMC	···	···	···	···	···	···	−5.15	···	···	···	···	···	···	2150	···	Disk signature
Sk −70 69	O5.5 V((f))	LMC	285	165	40500	3.7	3.73	9.6	−4.83	−3.79	5.35	18	35	0.8	0.8	2300:	0.10	Previously modeled
Sk −68 41	B0.5 Ia	LMC	270	150	24500	2.9	2.95	33.4	−6.71	−2.44	5.56	36	33	0.9	2.0	865	0.10	
Sk −69 124	O9.7 I	LMC	190	160	29250	3.1	3.15	21.3	−6.07	−2.88	5.48	23	32	0.7	1.2	1430	0.10	
BI 170	O9.5 I	LMC	290	150	31500	3.15	3.20	16.6	−5.66	−3.06	5.39	16	31	0.8	1.2	1370	0.15	
BI 173	08.5 II(f)	LMC	285	200	34500	3.4	3.45	17.6	−5.93	−3.31	5.60	32	40	1.6	0.8	1950:	0.10	
LH 64−16	ON2 III(f*)	LMC	290	150	53000	3.8	3.82	9.9	−5.23	−4.62	5.84	24	74	4.0	0.8	3250	0.50	Previously modeled
Sk −67 166	O4 If	LMC	290	180	39000	3.4	3.43	22.1	−6.54	−3.73	6.01	48	71	4.5	0.8	735	0.20	Previously modeled
BI 192	O9 III	LMC	300	140	32500	3.5	3.53	12.1	−5.03	−3.13	5.17	18	26	0.1	0.8	1100:	0.10	
BI 208	O6 V((f))	LMC	320	240	39500	3.8	3.85	9.88	−4.87	−3.71	5.33	25	34	0.3	0.8	980:	0.10	

Notes.
[a] From the nonrotating models of Charbonnel et al. (1993; SMC) and Schaerer et al. (1993; LMC).
[b] Units of 10^{-6} $M_\odot$ yr^{-1}. The true mass-loss rates will be these values corrected by $\sqrt{1/f}$, where f is the unknown "clumping" factor, probably of order 6–10 or less; see the recent workshop proceedings by Hamann et al. (2008).
[c] By number.

comparing the synthetic spectra with the observed spectrum. The β parameter (related to the acceleration of the stellar wind) and the He-to-H ratio were altered, if needed. Values for the metallicity $Z/Z_{\odot}$ of 0.2 (SMC) and 0.5 (LMC) were adopted as mentioned earlier, as we did in Papers I and II, respectively. We have scaled the solar abundance of Asplund (2003) by these factors rather than the (older) solar abundances used in Papers I and II, although the differences are in fact imperceptible. As we noted in Paper I, the actual relative abundances of the interstellar medium in the SMC, LMC, *and* the nearby regions of the Milky Way are nonsolar, as discussed by Westerlund (1997); hence this is not really the right thing to do, but lacking detailed abundance analysis of these stars (which is beyond the scope of this paper), this is the best we can do for now.

In general, certain lines were primarily affected by varying a single stellar parameter. For instance, the strengths of the model He I and He II lines were primarily sensitive to a change in $T_{\rm eff}$. The stars in our sample covered the range of effective temperatures from 29,250 to 53,000 K. At the lowest values for $T_{\rm eff}$, the strengths of the Si III and Si IV lines were also useful. In Papers I and II, we argued that the uncertainty in our effective temperatures was 1000 K, but in many cases our temperatures are more precisely determined, as the models are sensitive to temperature differences of 250–500 K.

The effective surface gravity $g_{\rm eff}$ (surface gravity reduced by the effects of centrifugal acceleration due to the rotation of the star) was fitted by comparing the wings of Hγ lines with those of the models, with wider lines (more pressure broadened) indicative of a larger value. Values for $\log g_{\rm eff}$ in our sample ranged from 2.9 for the most extreme supergiant to 4.2 for the most compact dwarf. We could detect differences in the line profile of Hγ by varying $\log g$ by 0.1 dex.

The determination of the mass-loss rates ($\dot{M}$) very strongly depended on the line profile of Hα and, to a lesser extent, Hβ and He II λ4686. The mass-loss rates measured ranged from 0.05×10^{-6} to 4.5×10^{-6} $M_{\odot}$ yr $^{-1}$. Models with lower mass-loss rates were generally sensitive to adjustments of 0.1–0.2 $\times 10^{-6}$ $M_{\odot}$ yr $^{-1}$, while the stars with the largest mass-loss rates were sensitive to adjustments of about 1×10^{-6} $M_{\odot}$ yr $^{-1}$. The Hα profile becomes insensitive to mass-loss rates below about 0.1×10^{-6} $M_{\odot}$ yr^{-1}, and the details of the numerical approach can dominate the results. Models with the highest mass-loss rates had both Hα and He II λ4686 in emission. Typically, lines in emission allowed a determination of β, the wind acceleration parameter, which otherwise was set at default to 0.8. We note that in accordance with Papers I and II, the mass-loss rate we determine is with the assumption of homogeneous stellar winds; the actual mass loss will be related to this by $\sqrt{1/f}$, where f is the clumping factor. This factor is likely to be of order 6–10 or less if the clumping properties of O stars in the Clouds are similar to those in the Milky Way (see, e.g., the recent conference workshop by Hamann et al. 2008).

We assumed a standard He-to-H ratio of 0.1, and this sufficed for most of our fitting. In a few cases, we found that we had to increase this value in order to obtain sufficiently strong He lines. We discuss these individual cases below.

In comparing the star's line profiles with those of the models, we of course had to correct for the radial velocity of the star and to broaden the model's lines to match the rotational velocity of the star. We used the width of several He II lines as a gage of the rotational velocity. Strictly speaking, much of this broadening was due to the instrumental resolution, which created a floor in our measurements of 140 km s^{-1}. Occasionally, we had to adjust either the radial velocity or $v \sin i$ values from our preliminary measurements to obtain better agreement.

In Table 3, we list the final adopted models for each star. We include several derived parameters. The *true* surface gravity is the *effective* surface gravity corrected for the effects of centrifugal acceleration due to the rotation of the star. This correction can be approximated (in a statistical sense, assuming randomly distributed rotational axis orientations) as simply the square of the projected rotational velocity divided by the stellar radius R:

$$g_{\rm true} = g_{\rm eff} + \frac{(v \sin i)^2}{6.96R},$$

following Repolust et al. (2004). As discussed above, we expect that low "rotational velocities" are actually dominated by the instrumental resolution, but these have a negligible effect. Even the highest rotational velocities in our sample (240 km s^{-1}) contribute only 0.05 dex to $\log g_{\rm true}$, as seen for BI 208 in Table 3. We also include an estimate of the spectroscopically derived mass of the star, based upon our determination of $\log g_{\rm true}$ and the stellar radius (since $M_{\rm spec} = g_{\rm true}/g_{\odot}R^2$, where the mass and radius are in solar units); we will compare these "spectroscopic" masses with those derived from evolutionary tracks using the star's effective temperature and luminosity in the next section.

We expect some significant number of stars in our sample of 26 stars to have no satisfactory fits, as some fraction will actually be composites of two (or more!) stars. At least 7 out of the 40 stars analyzed in Papers I and II admitted no good solution. In this way, our method has some significant advantages over the "automatic fitting method" of Mokiem et al. (2005, 2006, 2007), which obtains a "best answer" for every star (see discussion following de Koter 2008), but does not reject cases where the model is an unlikely match to the data (see discussion in Press et al. 1992).

Several of our stars have been previously analyzed, and we included these in our program as such overlap provides a crucial test of the methods (and data) of ourselves and others. In Tables 4 and 5, we include a comparison of the principal physical properties found by ourselves and others. In comparing these values, one should keep in mind that the effective temperature ($T_{\rm eff}$) and surface gravities ($\log g_{\rm eff}$) are not quite independent—in general, a *model* with 2000 K cooler temperature will require (roughly) a surface gravity that is 0.1 dex lower to preserve the shape of the Balmer line wings.

Throughout the following section, note that the scale of the figures showing the line profiles varies from line to line and star to star, as indicated by the labels. In a few very early-type O stars (i.e., LH 64−16 and Sk−67°166), the He I λ4471 line is the only He I we detect even with our 3σ limit of 12 m Å, and hence is the only He I line we used in the fitting, but we still show the comparison between the model and spectra for He I λ4387 and He I λ4922 lines for consistency. We also call attention to the fact that, with FASTWIND, the He I triplet λ4471 model line is often too weak for middle and late O-type giants and supergiants (Repolust et al. 2004). This so-called generalized dilution effect has been previously seen by others (e.g., Voels et al. 1989) and is not well understood. In this spectral range, we rely more on the strong singlet He I λ4387 line. In our experience, this line is quite well modeled by FASTWIND. Najarro et al. (2006) called attention to a problem that codes which treat line blanketing exactly (such as CMFGEN and TLUSTY) have with He I λ4387 and other singlets, probably due to some uncertainties in the atomic data of Fe IV lines overlapping with the He I resonance

Table 4
Comparisons of Current Sample with Previous Modeling

Type	$T_{\rm eff}$	log $g_{\rm eff}$	log $L/L_\odot$[a]	$\dot{M}$[b]	β	He/H[c]	Program	Ref.
				AzV 15				
O6.5 I(f)	38500	3.6	5.82	1.8	0.8	0.10	FASTWIND	This study
O7 II	39400	3.7	5.82	1.1	0.8	0.10	FASTWIND	6
O6.5 II(f)	37000	3.5	5.6	...	...	0.10	TLUSTY	1
				AzV 75				
O5.5 I(f)	39500	3.5	6.08	3.0	0.8	0.10	FASTWIND	This study
O5.5 I(f)	40000	3.6	6.18	3.5	0.8	0.10	FASTWIND	Paper I
O5 III(f+)	38500	3.5	5.9	...	...	0.10	TLUST	1
				AzV83				
O7 Iaf	...	...	...	...	...	...	FASTWIND	This study—binary?
O7 Iaf+	35000	3.25	5.5	...	...	0.20	TLUSTY	1
O7 Iaf+	32800	3.25	5.46	2.3[d]	2.0	0.20	CMFGEN	2
				NGC 346−324				
O5 V	42000	3.9	5.51	0.6	0.8	0.10	FASTWIND	This study
O4 V ((f+))	42800	3.9	6.02	0.2	0.8	0.08	FASTWIND	6—binary
O4 V ((f))	41500	4.0	5.44	0.3	1.0	0.10	TLUSTY /CMFGEN	3
O4 V ((f))	40000	3.7	5.46	$\leqslant$0.3	1.0	0.10	Nonblanketed models	4
				NGC 346−355				
O2 V	49500	3.9	5.95	2.0	0.8	0.10	FASTWIND	This study
ON2 III(f*)	52500	4.0	5.96	2.5	0.8	0.10	TLUSTY/CMFGEN	3
ON2 III(f*)	52500	4.0	5.99	1.6	1.0	0.10	CMFGEN	5
O3 III f*	55000	3.9	6.02	2.3	0.8	0.10	Nonblanketed models	4
				NGC 346−368				
O6 V	...	...	...	...	...	...	FASTWIND	This study—binary?
O4-5 V((f))	40000	3.8	5.34	0.2	1.0	0.10	TLUSTY/CMFGEN	3—binary?
				NGC 346−487				
O8 V	38000	4.2	5.19	0.1	0.8	0.10	FASTWIND	This study
O8 V	35000	4.0	5.08	<0.1	1.0	0.10	TLUSTY/CMFGEN	3
				NGC 346−682				
O8 V	36000	4.1	4.97	0.05	0.8	0.10	FASTWIND	This study
O9 V	36800	4.2	4.95	1.1	0.8	0.10	FASTWIND	6
O9-O9.5 V	32500	3.75	5.0	...	...	0.1	TLUSTY	1
				AzV 232				
O7 Iaf+	...	...	...	...	...	...	FASTWIND	This study—binary?
O7 Iaf+	34100	3.4	6.02	6.0	1.2	0.24	FASTWIND	6
O7 Iaf+	32000	3.1	5.85	4.5	1.65	0.2	CMFGEN	7
O7 Iaf+	37500	3.2	6.11	5.5	1.4	0.20	Nonblanketed models	4
				AzV 327				
O9.7 I	30800	3.2	5.6	0.7	0.8	0.15	FASTWIND	This study
O9.5 II-Ibw	30000	3.25	5.3	...	...	0.1	TLUSTY	1
				AzV 388				
O5.5 V ((f))	42500	3.9	5.53	0.3	0.8	0.10	FASTWIND	This study
O4 V	43000	3.9	5.55	0.33	0.8	0.09	FASTWIND	6
O4 V	48000	3.70	5.66	0.17	1.0	0.10	Nonblanketed models	4
				Sk−70°69				
O5.5 V((f))	40500	3.7	5.35	0.8	0.8	0.10	FASTWIND	This study
O5 V	43200	3.9	5.41	1.1	0.78	0.17	FASTWIND	8
				LH 64−16				
ON2 III(f*)	53000	3.8	5.84	4.0	0.8	0.50	FASTWIND	This study
ON2 III(f*)	54500	3.9	5.86	4.0	0.8	0.60	FASTWIND	Paper I
ON2 III(f*)	55000	4.0	5.90	1.6	1.0	0.25	CMFGEN	5
				Sk −67°166				
O4 If	39000	3.8	6.01	4.5	0.8	0.20	FASTWIND	This paper
O4 Iaf+	40300	3.7	6.03	9.3	0.9	0.28	FASTWIND	8
O4 If*	47500	3.6	6.24	13.0	0.7	0.10	Nonblanketed models	4

Notes.
[a] Corrected to a true DM of 18.9 (60.3 kpc) for the SMC. Previous studies of LMC stars have assumed the same true DM as we do, 18.5 (50.1 kpc).
[b] In units of 10^{-6} $M_\odot$ yr^{-1}. These are all for "unclumped" (homogeneous) stellar winds.
[c] By number.
[d] Corrected to an "unclumped" wind mass-loss rate by the factor of 3.3.
References. (1) Heap et al. (2006); (2) Hillier et al. (2003); (3) Bouret et al. (2003); (4) Puls et al. (1996); (5) Walborn et al. (2004); (6) Mokiem et al. (2006); (7) Crowther et al. (2002); (8) Mokiem et al. (2007).

Table 5
Comparisons of Other Stars with Previous Modeling

Type	$T_{\rm eff}$	$\log g_{\rm eff}$	$\log L/L_{\odot}$	$\dot{M}^{a}$	β	He/H[b]	Program	Ref.
				AzV 14				
O5 V	44000	4.0	5.85	0.1	0.8	0.10	FASTWIND	Paper I
O5 V	45300	4.1	5.86	0.3	0.8	0.10	FASTWIND	1
				AzV 26				
O6 I(f)	38000	3.5	6.14	2.5	0.8	0.10	FASTWIND	Paper I
O7 III	40100	3.8	6.17	1.7	0.8	0.09	FASTWIND	1
				AzV372				
Binary	...	...	...	...	...	...	FASTWIND	Paper 1—Binary
O9Iabw	31000	3.2	5.83	2.0	1.3	0.11	FASTWIND	1
				AzV 469				
O8.5 I(f)	32000	3.1	5.64	1.8	0.8	0.20	FASTWIND	Paper I
O8 II((f))	34000	3.4	5.70	1.1	1.2	0.17	FASTWIND	1
				BI 237				
O2 V((f*))	48000	3.9	5.77	2.0	0.8	0.10	FASTWIND	Paper II
O2 V((f*))	53200	4.1	5.83	0.8	1.3	0.10	FASTWIND	2
				BI 253				
O2 V ((f*))	>48000	3.9	>5.77	3.5	0.8	0.10	FASTWIND	Paper II
O2 V ((f*))	53800	4.2	5.93	1.9	1.2	0.09	FASTWIND	2

Notes.
[a] In units of 10^{-6} $M_{\odot}$ yr^{-1}. These are all for "unclumped" (homogeneous) stellar winds.
[b] By number.
References. (1) Mokiem et al. (2006); (2) Mokiem et al. (2007).

lines around 584 Å. With its approximate treatment of line blanketing and blocking, FASTWIND should be less sensitive to this issue, but future comparisons with other codes are needed to fully resolve this issue.

3.4. Individual Stars

3.4.1. SMC

AzV 15. Visually, we would classify this star as O6.5, given the relative strengths of the He I and He II lines (Figure 1, upper panel). The measured EW of He I λ4471 is 430 mÅ and that of He II λ4542 is 660 m Å, leading to $\log W' = -0.19$, also indicative of an O6.5 type. N III λλ4634, 42 is strong in emission, whereas He II λ4686 is in absorption. This combination would lead to a "(f)" designation, which (at Milky Way metallicity) is associated with the star being of luminosity class III for an O6.5 star. However, the corresponding absolute magnitude is −6.15, more in keeping with it being a supergiant. This is similar to what we found for a number of SMC stars in Papers I and II—the weaker stellar wind (due to the lower metallicity of the SMC) results in He II λ4686 being in absorption for stars of a given M_V and spectral type that, had they been found in the Milky Way, would have had He II λ4686 in emission. At our high S/N, we detect very weak Si IV λ4116 emission (−50 m Å EW), although Si IV λ4089 is weak in absorption (40 m Å EW). Strong Si IV λλ4089, 4116 emission is associated with earlier types in Milky Way stars, but our high S/N apparently allows detection in later types, as discussed above. It may also be that, at lower metallicity, it will be in emission at somewhat later types. We note in passing that the current models do not correctly reproduce the behavior of these lines, not even for extreme Galactic examples where the lines are in strong emission.

We describe this star as O6.5 I(f), a designation that would be an oxymoron were it to be applied to a Galactic star. The star had previously been called an O7 II by Garmany et al. (1987) and an O6.5 II(f) by Heap et al. (2006), both in substantial agreement with our designation. Of course, an alternative possibility would be that the star is composite; however, the fits for this star are very good (Figure 1, lower panel). We emphasize that fitting individual spectral lines is a very sensitive way to detect composite spectra—only if both components have very similar effective temperatures and luminosities would we likely be able to find a satisfactory fit to both the He I and He II lines at the same time. The star was previously modeled (Table 4) by Mokiem et al. (2006), who obtained an effective temperature 900 K higher than ours, and by Heap et al. (2006), who obtained an effective temperature 1500 K lower than ours.

AzV 61. The spectral subtype is O5.5, with EWs of 300 m Å (He I λ4471) and 750 m Å (He II λ4542), leading to $\log W' = -0.40$. The strength of N III λλ4634, 42 emissions would lead us to conclude that this star is a giant, but again we find that He II λ4686 is strong in absorption, more consistent with a dwarf. The absolute magnitude M_V we derive is −5.8, also consistent with the star being a giant, and we thus refer to this star as an O5.5 III((f)). Previously, the star had been called an O5 V by Crampton & Greasley (1982). The blue spectrum in shown in Figure 2 (upper panel).

We were unable to obtain a satisfactory fit to this star, primarily due to the fact that Hα is strong in emission and double-peaked (Figure 2, lower panel), while He II λ4686 is strong in absorption, as shown in the upper panel. Hβ is also filled in with emission. Either this star is a binary or it is surrounded by a circumstellar disk, as we suspect is the case for two stars discussed below.

AzV 75. The spectrum in shown in Figure 3 (upper panel). The spectral subtype is O5.5, based both upon the visual appearance and the measurements of EWs (335 m Å for He I λ4471 and 680 m Å for He II λ4542, leading to $\log W' = -0.31$). N III λλ4634, 42 is strong in emission, consistent with the star being a supergiant. He II λ4686 is in (weak) absorption, which would lead to a giant luminosity class. Again, we find that the absolute magnitude ($M_V = -6.7$) is consistent with the star being a supergiant, so we again call this an O5.5 I(f).

The star was included in Paper I, where we independently called it an O5.5 I(f). However, here we note very weak

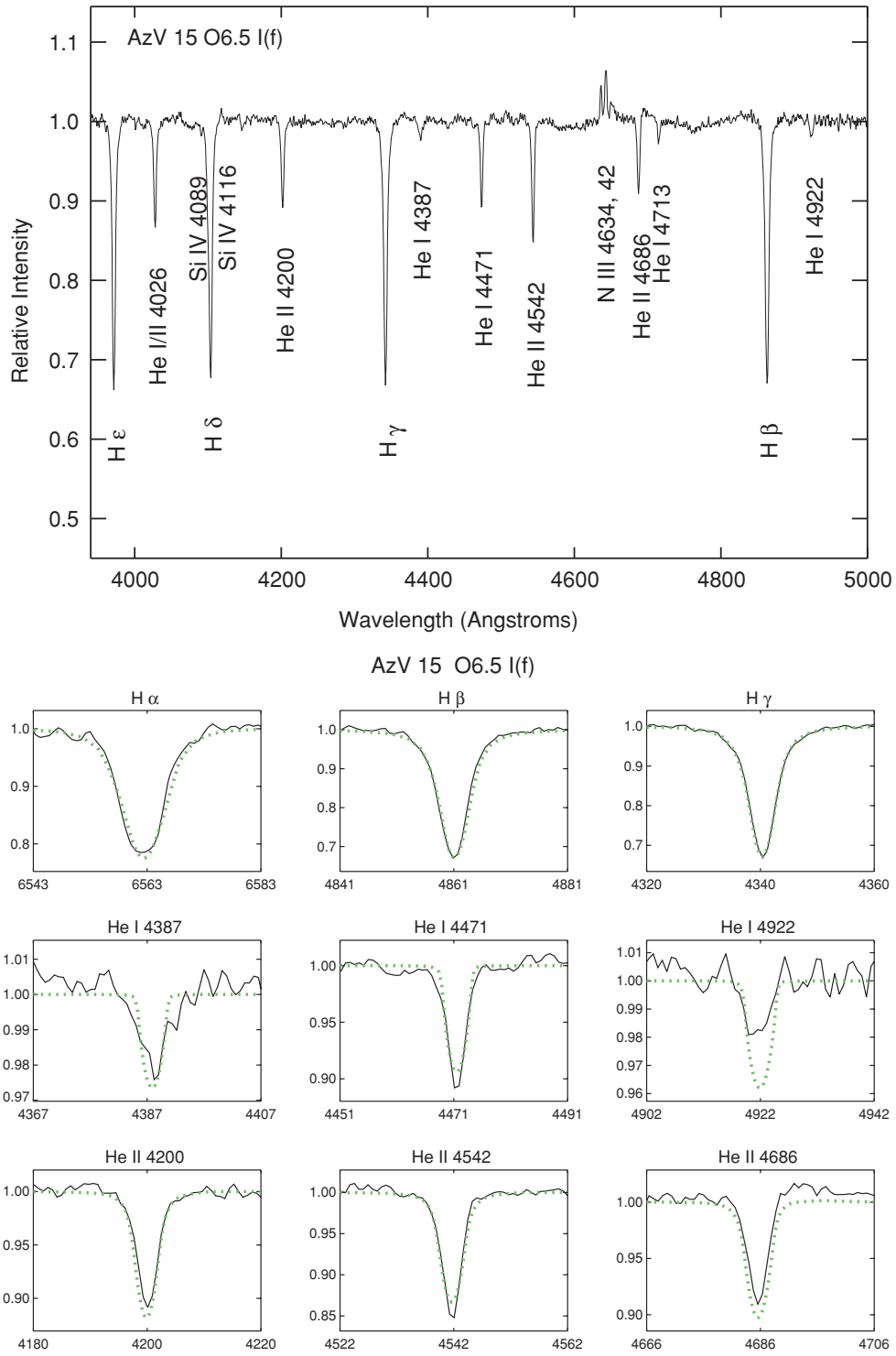

Figure 1. AzV 15. The upper figure shows a section of the blue spectrum of this star, with the prominent lines identified. The lower figure shows the fits (dotted) for the principal diagnostic lines.

(A color version of this figure is available in the online journal.)

N IV λ4058 emission and possible Si IV λ4116 emission. Heap et al. (2006) referred to this star as an O5.5 III(f+), with "+" indicating that they recognized the Si IV emission as well. The presence of emission lines of N IV and Si IV could be an indication that the spectrum is composite, as these emission lines are usually associated with earlier spectral types. However, as we discussed above, the emission mechanisms involved may result in these lines not having the same connection with spectral types as in the Milky Way.

The fits we obtained for this star were reasonably good (Figure 3, lower panel). The He I λ4471 model line is a little weak, but that is consistent with the fact that FASTWIND (and likely other models) does not seem to produce a strong enough He I λ4471 line for supergiants and giants of this type and later. The model He I λ4922 is a good match, but He I λ4387 is a bit weak. We found that if we lowered the effective temperature by 500–1000 K, the agreement with He I λ4387 improved, but that both He I λ4922 and He I λ4713 (not shown) got too strong in

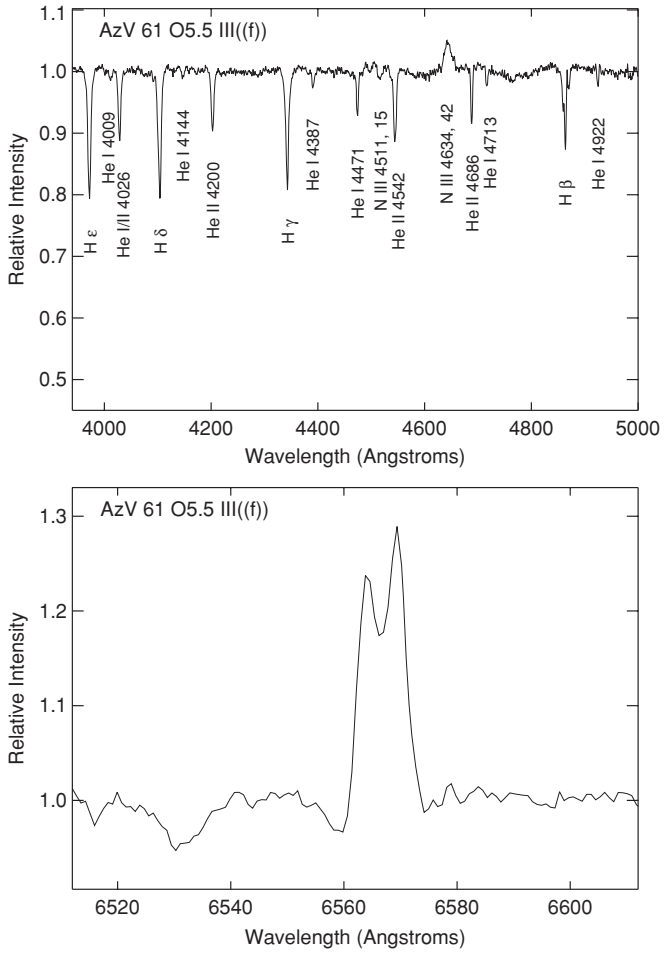

Figure 2. AzV 61. The upper figure shows a section of the blue spectrum of this star, with the prominent lines identified. The lower figure shows the Hα profile.

the models; so we adopted the hotter fit. Our model fits were done without reference to Paper I. Nevertheless, the agreement is excellent, as shown in Table 4. Heap et al. (2006) also analyzed this star and derived an effective temperature 1000 K cooler than what we do here.

AzV 83. The spectrum is shown in Figure 4. The spectral subtype for this star is O7, based on both its visual appearance and the EW measurements (660 m Å for He I λ4471 and 680 m Å for He II λ4542, leading to $\log W' = -0.01$). Both N III λλ4638, 42 and He II λ4686 are strong in emission, leading to an "If" luminosity class or even an "Iaf" class, given the strength of emission. Yet $M_V = -6.18$ is intermediate between a giant and a supergiant. N IV λ4058 and Si IV λλ4089, 4116 are in weak emission, similar to AzV75, although Si IV is more strong in emission than in AzV75. The star was analyzed by Hillier et al. (2003), who also called it an O7 Iaf+, although this extreme luminosity classification is somewhat at variance with the absolute visual magnitude. Si IV emission is present in the Hillier et al. (2003) spectra and is also present (weakly) in the final adopted model. N IV λ4058 is shown to be weak in emission in their spectra, although their final adopted model has this line weak in absorption. The star was also analyzed by Heap et al. (2006).

Despite having examined over 80 models, we were unable to obtain a satisfactory fit to the spectrum of this star. Our best solution required an effective temperature in the neighborhood of 36,000–38,000 K in order to match the weakness of the He I λ4387 line, and we also required a He/H value of 0.2 to obtain sufficiently strong He II absorption in a reasonable temperature regime. Yet such a high temperature is inconsistent with the Si IV UV P Cygni profile (D. J. Hillier 2008, private communication). As shown in Table 4, Hillier et al. (2003) derived a much lower temperature, 32,800 K, while Heap et al. (2006) found an intermediate temperature (35,000 K). As Heap et al. (2006) emphasized, the temperatures derived for this star depended in large part upon which He I lines are given the stronger weight in the fit, as the results are inconsistent. We note the following. (1) The absolute visual magnitude, $M_V = -6.18$, is considerably fainter than what we would expect for such an "extreme" Of star; it is more in keeping with a normal supergiant. (2) The O7 Iaf star AzV232 (discussed below) has *weaker* luminosity indicators and yet has $M_V = -6.96$. This is hard to understand if both of these are single stars. However, if the N III λλ4634, 42 and He II λ4686 emissions were primarily from a hotter component in AzV 83, this would make sense, although the sum of the stars' luminosities would still have to be no larger than that of a single supergiant. Also, the terminal velocity determined from the UV lines is consistent with a supergiant, and there is no evidence of the faster wind which we would associate with a dwarf—any composite explanation would have to satisfy both the optical and the UV spectra. Still, although we do not see a significant radial velocity difference ($\Delta v_r < 30$ km s^{-1}) between the adjacent nights on which our spectra (blue and red) were obtained, we believe that a radial velocity study might be useful.

NGC 346−324. The spectrum is shown in Figure 5 (upper panel). We assign a spectral subtype of O5 for this star, based on both its overall visual appearance and the measured EWs of He I λ4471 and He II λ4542 (250 m Å and 760 m Å, respectively), leading to $\log W' = -0.48$. There is no N III λλ4634, 42 or He II λ4686 emission, which would suggest a "V" luminosity class. The absolute visual magnitude is −5.13, also quite consistent with the "V" class. The star has been classified as an O4 V((f)) by both Massey et al. (1989) and Walborn et al. (2000), but we are satisfied with our slightly later classification. Niemela et al. (1986) called the star an O4–5 V. The spectra have some nebular contamination, as judged by the oversubtraction of [O III] λ4959 and λ5007. Weak N IV λ4058 (EW = −100 m Å) is also present, as is very weak Si IV λ4116 emission (EW = −25 m Å). Again, such features would go undetected at lesser S/Ns.

The fits we obtained were good (Figure 5, lower panel): He I λ4471 is little too strong in our adopted model, as is He II λ4200. Other lines show excellent agreement. The star has been previously analyzed by Bouret et al. (2003) and Puls et al. (1996); the agreement in Table 4 is quite good, despite the differences in code and data used in these studies.

The star was included in the "automated" fitting program of Mokiem et al. (2006), who obtained results nearly identical to ours (Table 4). They added a footnote to their Table 1 suggesting that this star is a binary, based apparently on variable radial velocities although Mokiem et al. (2006) cryptically noted that none of their three detected binaries "appear to have massive companions," and hence concluded that their derived fitting parameters are valid. They did not quote any radial velocities. The star has also been analyzed by Heap et al. (2006), again with very similar results.[10]

[10] Mokiem et al. (2006) stated that their effective temperature for this star differs significantly from that derived by Heap et al. (2006), but quoted an effective temperature that corresponds to a different NGC 346 star studied by Heap et al. (2006). The agreement for this star is actually reasonably good.

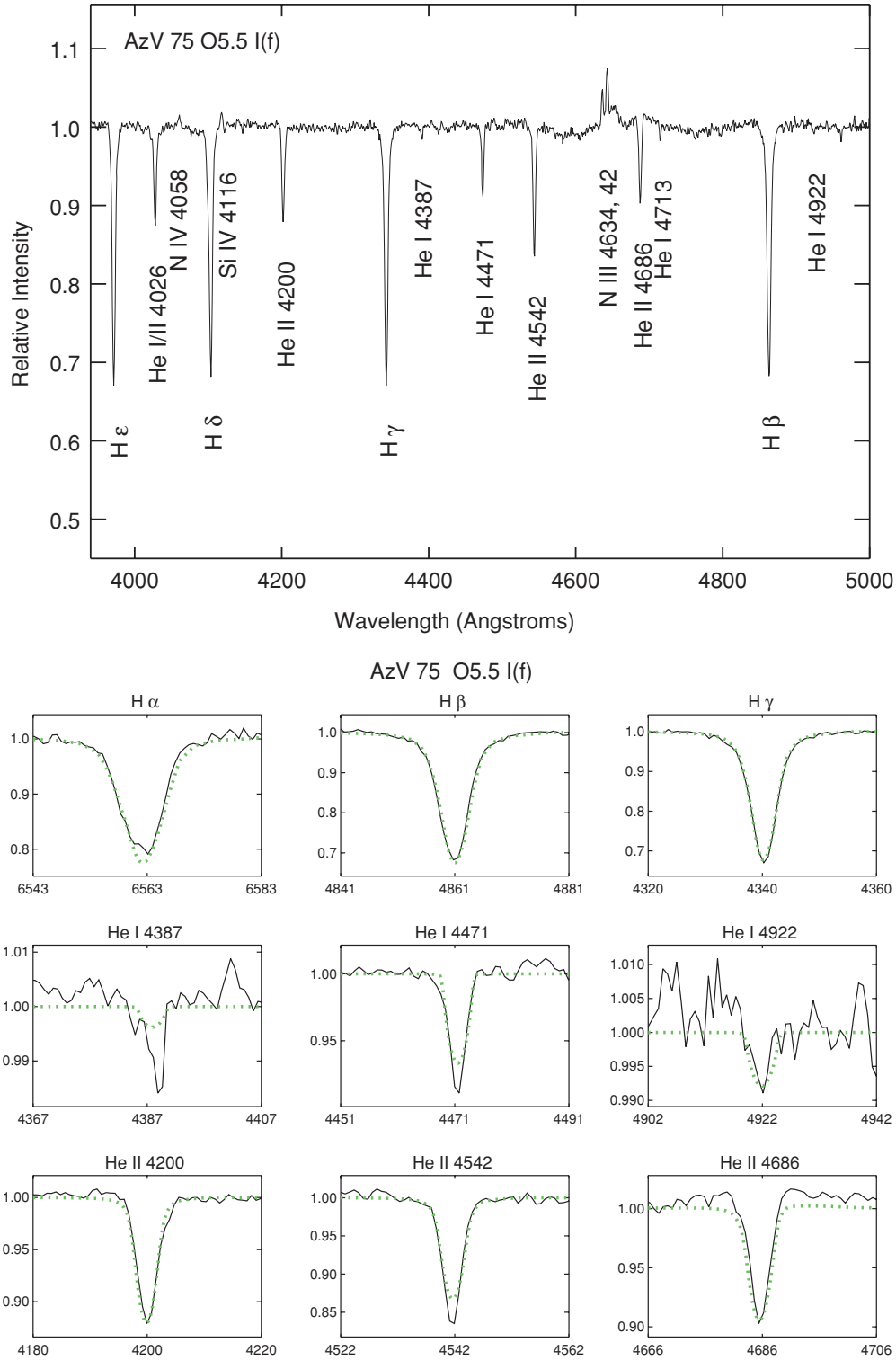

Figure 3. AzV 75. The upper figure shows a section of the blue spectrum of this star, with the prominent lines identified. The lower figure shows the fits (dotted) for the principal diagnostic lines.

(A color version of this figure is available in the online journal.)

NGC 346−342. The spectrum is shown in Figure 6. We obtain a spectral subtype of O5.5 for this star, based on its general appearance and the measured EWs (410 m Å for He I λ4471 and 850 m Å for He II λ4542), leading to log $W' = -0.32$. N III λλ 4634, 42 is in emission but He II λ4686 is in absorption, and we might call this an O5.5 V ((f)), as did Massey et al. (1989), but the absolute magnitude is −5.52, more like that of a giant. We would, therefore, call this star an O5.5 III((f)). However, we conclude that the star is composite. First, we were unable to obtain consistent fits to the He I and He II lines. Second, close examination of the spectrum revealed an inflection point on the He I lines suggesting incipient double lines. Third, and

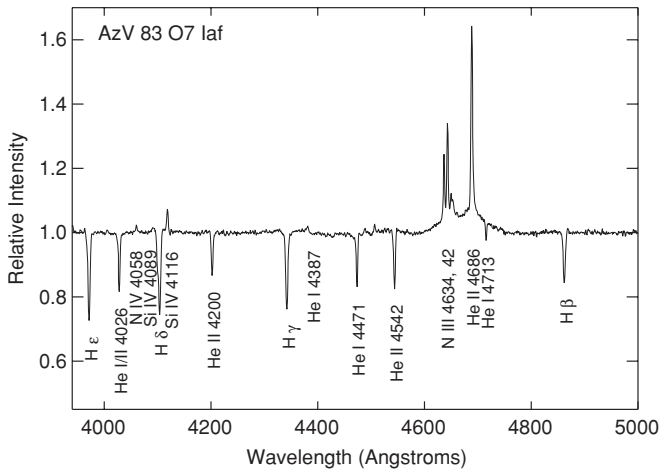

Figure 4. AzV 83. The figure shows a section of the blue spectrum of this star, with the prominent lines identified.

most convincingly, the star has been found to be an eclipsing binary in data obtained by three of the coauthors (P.M., N.I.M., K.D.E.) in connection with another project. These data show eclipses of 0.25 mag and a period of 2.35 days. A follow-up spectrum obtained in January revealed clear double lines, with spectral types of O5 V and O7 V, with some indication of a third component, which has now been confirmed by additional spectroscopy at Magellan. A follow-up radial velocity study is in progress.

NGC 346−355. The spectrum is shown in Figure 7 (upper panel). It is the earliest type star in our sample, and indeed is offered by Walborn et al. (2002) as a representative of the earliest defined spectral class, O2. Walborn et al. (2002) assigned a luminosity class of III(f*). We measure an EW of 40 ± 10 m Å for He I λ4471 in our spectrum, consistent with what we found in Papers I and II and also with the statement by Walborn et al. (2002) that O2 giants and supergiants show "no or very weak" He I. The EW of He II λ4542 is 720 m Å. For the earliest type stars Walborn et al. (2002) proposed a classification scheme based on the relative strengths of the N IV and N III emission lines, and consistent with our find that N IV λ 4058 is much stronger than N III λλ 4634,42 emission.

The effective temperature of our final model (Figure 7, lower panel) is strongly constrained by the weak He I λ4471 we measure, as the strengths of the He II lines are no longer sensitive to changes of effective temperatures in this regime. Over the range 48,500–50,500 K, the EW of He I λ 4471 changes from 51 to 23 m Å, which may be compared with 40 ± 10 m Å we measure. Our effective temperature for this star is significantly lower than others in the literature (Table 4), which is necessitated by the (very weak) He I λ4471 we detect. At 52,500 (found by Bouret et al. 2003 and Walborn et al. 2004 from the data described by Walborn et al. 2000), the expected EW of He I λ4471 is only 8 m Å, inconsistent with what we find with our higher S/N data.

There is some incomplete nebular subtraction of the [O III] lines, and we see residual emission in the Hα profile which we attribute to nebulosity despite our careful sky (and nebular) subtraction.

NGC 346−368. The spectrum is shown in Figure 8. It shows a (composite) spectral type of O6, with an EW of He I λ4471 of 380 m Å and an EW of He II λ4542 of 750 m Å, yielding $\log W' = -0.30$. N III λλ4634, 42 is evident in emission but He II λ4686 is strong in absorption, suggesting a luminosity class of "V((f))," consistent with the measured absolute magnitude $M_V = -5.0$. However, when we measured the radial velocities of the lines, we found a significant difference (50 km s^{-1}) between the values for He I and He II. The star shows no light variations in the eclipsing binary search alluded to above, but we conclude that it is likely a binary. We attempted a few fits, but found nothing satisfactory.

The spectrum was modeled by Bouret et al (2003), who called the star an O4–5 V((f)), considerably earlier than what we find here for the composite type or for the O6 V((f)) type found by Massey et al. (1989). Heap et al. (2006) gave further details of this fitting, noting that the radial velocities from the UV spectrum and optical disagreed by 70 km s^{-1}, and suggesting that the star might be a binary. Nevertheless, they included their analysis of this star in their effective temperature compilation.

NGC 346−487. The spectrum of this star is shown in Figure 9 (upper panel). Visually, the spectral subtype is O8, as He I λ4471 is slightly stronger than He II λ4542. We measure EWs of 790 m Å and 615 m Å, respectively, leading to $\log W' = +0.11$, also indicative of an O8 type. He II λ4688 is strong in absorption, and there is no N III λλ4638, 42 emission, and so we call this an O8 V, which is also in accord with $M_V = -4.6$. The star was classified quite a bit earlier, O6.5 V, by Massey et al. (1989). Our fits, shown in Figure 9 (lower panel), were good.

The star was also analyzed by Bouret et al. (2003), who derived an effective temperature 3000 K cooler than our result, along with a significantly (0.2 dex) smaller value for $\log g$ (Table 4). Their values were primarily derived from the UV, as they were unable to obtain a satisfactory fit to the optical without assuming an unlikely low value for the metallicity. They concluded that their optical spectrum was contaminated by other stars on the slit. Below, we argue that the problem with their optical data was moonlight contamination, and compare their data with ours (Section 4.1).

AzV 223. We show the spectrum of this star in Figure 10 (upper panel). The He I λ4471 line (EW of 950 m Å) is much stronger than He II λ4542 (EW of 250 m Å), leading to an O9.5 type ($\log W' = 0.58$). He II λ4200 is still reasonably strong (EW of 285 m Å) and so we were not tempted to call this a B0, although others might call it an O9.7 type. Were this a Galactic star, we would call the luminosity class "V" or "III" based on the strength of He II λ4686 absorption. However, the absolute magnitude $M_V = -5.6$ is more intermediate between a "III" and a "I." Given the expected weakness of the wind lines in the SMC, we adopt an O9.5 II classification for this star. Previously, the star was classified as O9 III by Garmany et al. (1987). The fits we obtained are quite good, and are shown in Figure 10 (lower panel).

NGC 346−682. The spectrum is shown in Figure 11 (upper panel). We measure EWs of 810 m Å and 530 m Å for He I λ4471 and He II λ4542, respectively, leading to $\log W' = +0.18$, consistent with the O8 subtype suggested by the visual appearance. We conclude that the star is a dwarf, based upon the strong He II λ4686 absorption and the fact that $M_V = -4.2$. Our O8 V type is identical to that found by Massey et al. (1989).

The model for this star gave good agreement with the observed spectrum (Figure 11, lower panel). The star had been previously modeled both by Mokiem et al. (2006) and Heap et al. (2006). As can be seen in Table 4, the FASTWIND optical results (both ours and Mokiem et al. 2006) give somewhat higher

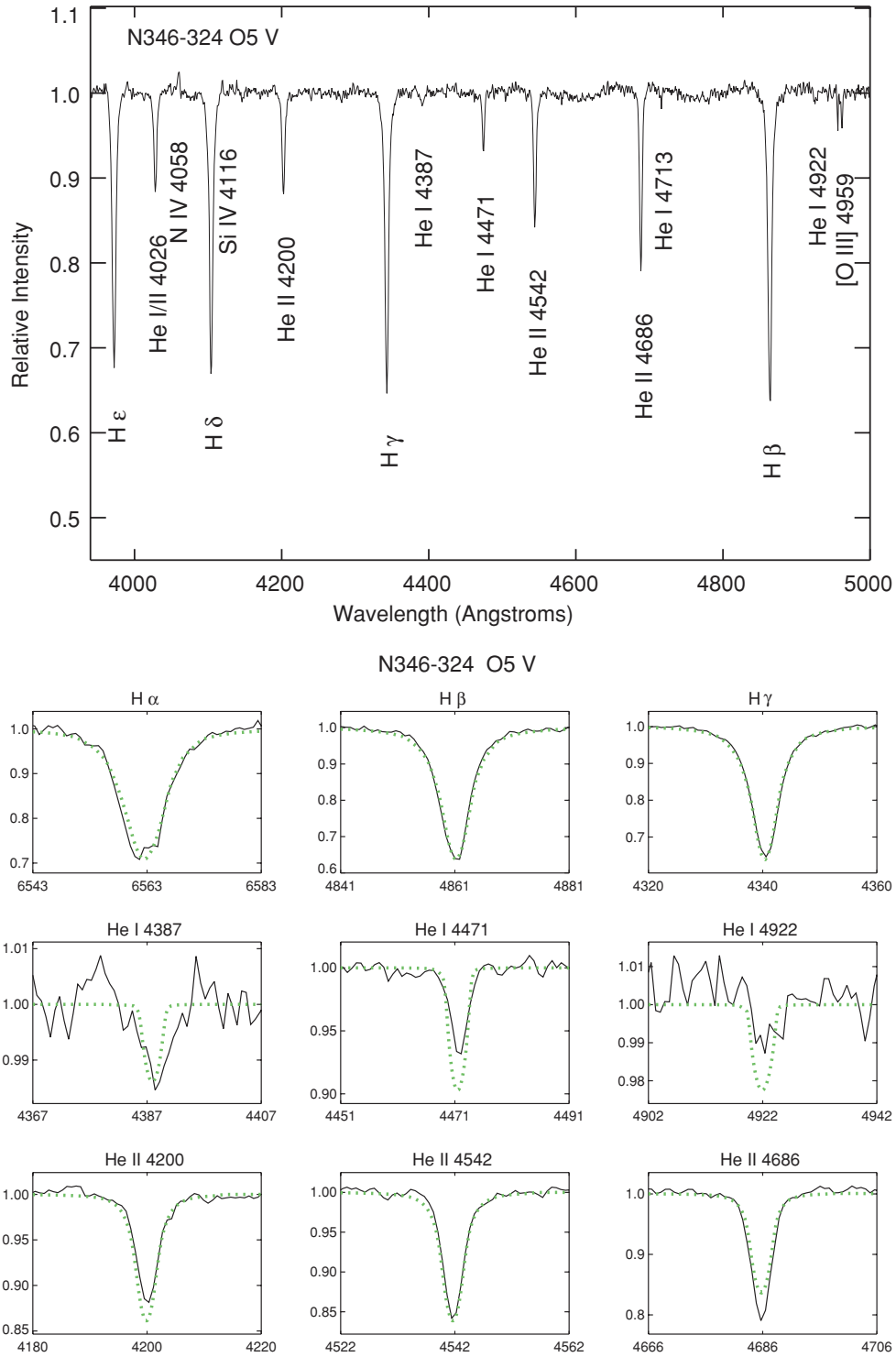

Figure 5. NGC 346−324. The upper figure shows a section of the blue spectrum of this star, with the prominent lines identified. The lower figure shows the fits (dotted) for the principal diagnostic lines.

(A color version of this figure is available in the online journal.)

temperatures and larger values for $\log g$ than the TLUSTY analysis by Heap et al. (2006).

AzV 232. This star, also known as Sk 80, is a well known O7 Iaf+ star (see, e.g., Walborn & Fitzpatrick 1990), a classification that we do not dispute. Our spectrum is shown in Figure 12. We measure EWs of 610 m Å and 680 m Å for He I λ4471 and He II λ4542, respectively; $\log W' = -0.05$, consistent with the O7 designation. The star has extremely strong N III λλ4638, 42 and He II λ4686 emission. Note that the Si IV λ4116 emission is considerably stronger than that of Si IV λ4089. We noticed this in a number of our spectra; this inequality is visible in Figure 5 of the Walborn & Fitzpatrick (1990) atlas and is even more obvious in our higher S/N spectrum.

Extreme supergiants are often hard to fit, but in this case we were completely stymied after 40 models. Even by significantly increasing the fractional He ratio, we could not

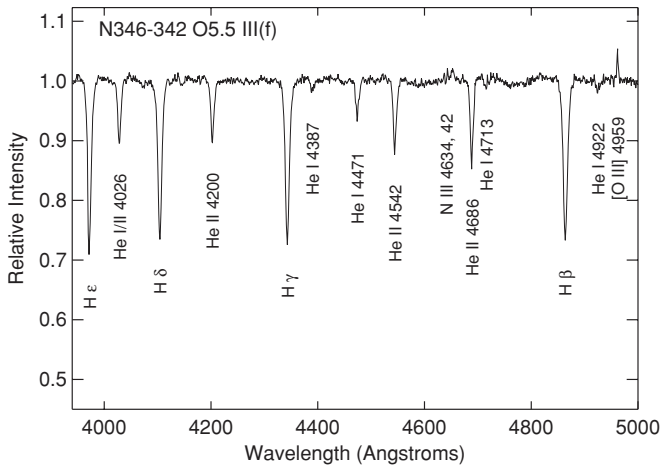

Figure 6. NGC 346−342. The figure shows a section of the blue spectrum of this star, with the prominent lines identified.

obtain sufficiently strong He I or He II lines. Mokiem et al. (2006) described this star as a binary based on radial velocity variations, although their automatic fitting procedure arrived at some "best-fit" properties, given in Table 4. The star was also successfully modeled by Crowther et al. (2002), who derived a cooler temperature (32,000 K vs. 34,100 K) than Mokiem et al.'s (2006) and a somewhat lower surface gravity (3.1 vs. 3.4).

AzV 327. This star is a late-type O supergiant, as evidenced by weak He II and strong He I, sharp and deep lines, and strong metal lines, such as Si IV and N III (Figure 13, upper panel). We measure EWs of 905 and 240 m Å for He I λ4471 and He II λ4542, respectively, leading to $\log W' = 0.58$, making this at least O9.5 or later. A B0 I is precluded by the strength of He II (especially, say, He II λ4200), but the strength of the Si IV features led us to use the intermediate spectral type O9.7 I as the spectrum closely resembles that shown for μ Nor by Walborn & Fitzpatrick (1990). The star had been previously classified as O9 I by Massey et al. (2000) and is listed as "O9.5 II-Ibw" by Walborn et al. (2000).

We obtained very nice fits for this star (Figure 13, lower panel), although it was necessary to use a slightly elevated He/H ratio (0.15) in order to make the He lines (both He I and He II) strong enough. The star has been previously modeled by Heap et al. (2006), who derived very similar parameters (Table 4). They found that the star had enriched N.

AzV 388. This star is a mid–early O star, with a visual type of O5.5 (Figure 14, upper panel). We measure EWs of 325 m Å and 800 m Å for He I λ4471 and He II λ4542, respectively, leading to $\log W' = -0.39$, or an O5.5 subtype. N III λλ4634, 42 shows weak emission, but He II λ4686 is strong in absorption. The absolute magnitude is −5.15 (Table 1). All of this is consistent with a dwarf luminosity class, and we call the star O5.5 V((f)). The star was previously classified as O4 V by Garmany et al. (1987) and Walborn et al. (1995).

The fits are quite good, and are shown in Figure 14 (lower panel). The star had been previously modeled by Mokiem et al. (2006) using a similar version of FASTWIND, with nearly identical results (Table 4).

3.4.2. LMC

BI 9. This star appears to be a mid-O dwarf or giant (Figure 15). We measure EWs of 670 m Å and 650 m Å for He I λ4471 and He II λ4542, respectively, leading to $\log W' = +0.01$, or an O7.5 subtype. N III λλ4634, 42 is strong in emission. This would suggest that the star is a giant, but He II λ4686 is strong in absorption. Were this star in the SMC, with its lower metallicity, we would attribute the behavior of He II λ4686 purely to the weaker stellar winds we expect. A giant luminosity class is consistent with the absolute magnitude, −5.8, but we were distrustful of the strong He II λ4686, which suggests that perhaps this star is a binary. We are forced to call this star an O7.5 III((f)). It was called an O8 III by Crampton (1979).

Our best-fit models have $\log g = 3.5$ and $T_{\rm eff}$ =36,000–36,250 K. However, we noticed that while the He I lines required $v \sin i \sim 180$ km s^{-1}, the He II lines were substantially broader, with apparently $v \sin i \sim 250$ km s^{-1}. The situation is reminiscent of P.M.'s first foray into the study of massive stars, the study of HDE 228766 (Massey & Conti 1977). There, Walborn (1973) had asserted that the He I lines were broad and the He II lines were sharp. This led to the first double-lined spectroscopic orbit for this interesting star. Here, we take the converse situation (He I narrow and He II broad) as an equally valid indicator that the star is likely a binary.

LMC 054383. This star was included in our program because an earlier spectrum, obtained with the fiber positioner Hydra, showed very weak hydrogen lines compared to He II lines, and we had described its spectrum to several colleagues as being a H-poor O3 star. However, with the higher S/N, long-slit spectrum we obtained here, we find that the hydrogen and He I lines are simply filled in by emission (Figure 16, upper panel). Furthermore, the emission is double-peaked. This is most clearly evident in the Hα emission profile (Figure 16, lower panel). The obvious interpretation is that the star is surrounded by a disk of material. Note that this spectrum is not that of a classical "Oe" star since N III λλ4634, 42 is also in emission; the spectral type is early, possibly an O4–O5 given the amount of He I absorption that we see. Given its absolute visual magnitude (−4.83) we call this an O4–O5V((f))pec. We made no attempt to model the star's spectrum.

Sk–70°60. Oddly, this star is very similar to that of LMC 054383, with both Balmer and He I lines showing double-peaked emission. The spectral type is early, O4–O5V((f))pec. The blue spectrum is shown in Figure 17 (upper panel) and the Hα profile in Figure 17 (lower panel). Again, no attempt was made to model the star.

Sk−70°69. This is an early O dwarf (Figure 18, upper panel), and we measure EWs of 340 m Å and 870 m Å for He I λ4471 and He II λ4542, respectively, leading to $\log W' = -0.41$, an O5.5 subtype. N III λλ4634, 42 emission is expected even in a dwarf at these early types, and He II λ4686 is strong in absorption, suggesting a dwarf luminosity class. The absolute magnitude −4.83 is also consistent with a dwarf, and so we call this star an O5.5 V((f)).

The fits we obtained for this star were excellent (Figure 18, lower panel). The star has also been analyzed by Mokiem et al. (2007), who found a higher effective temperature and somewhat higher values for the surface gravity and He/H content (Table 4).

Sk−68°41. This is an early-type B supergiant (Figure 19, upper panel), the latest star in our sample. We classify it as B0.5 Ia, based upon visual comparison with the Walborn & Fitzpatrick (1990) atlas. Our classification is based on the fact that Si IV λλ4089, 4116 absorption is about equal in strength to the strongest Si III λ4552 line, the (near) lack of He II absorption, the strength of the O II lines, and the weakness of Mg II λ4481.

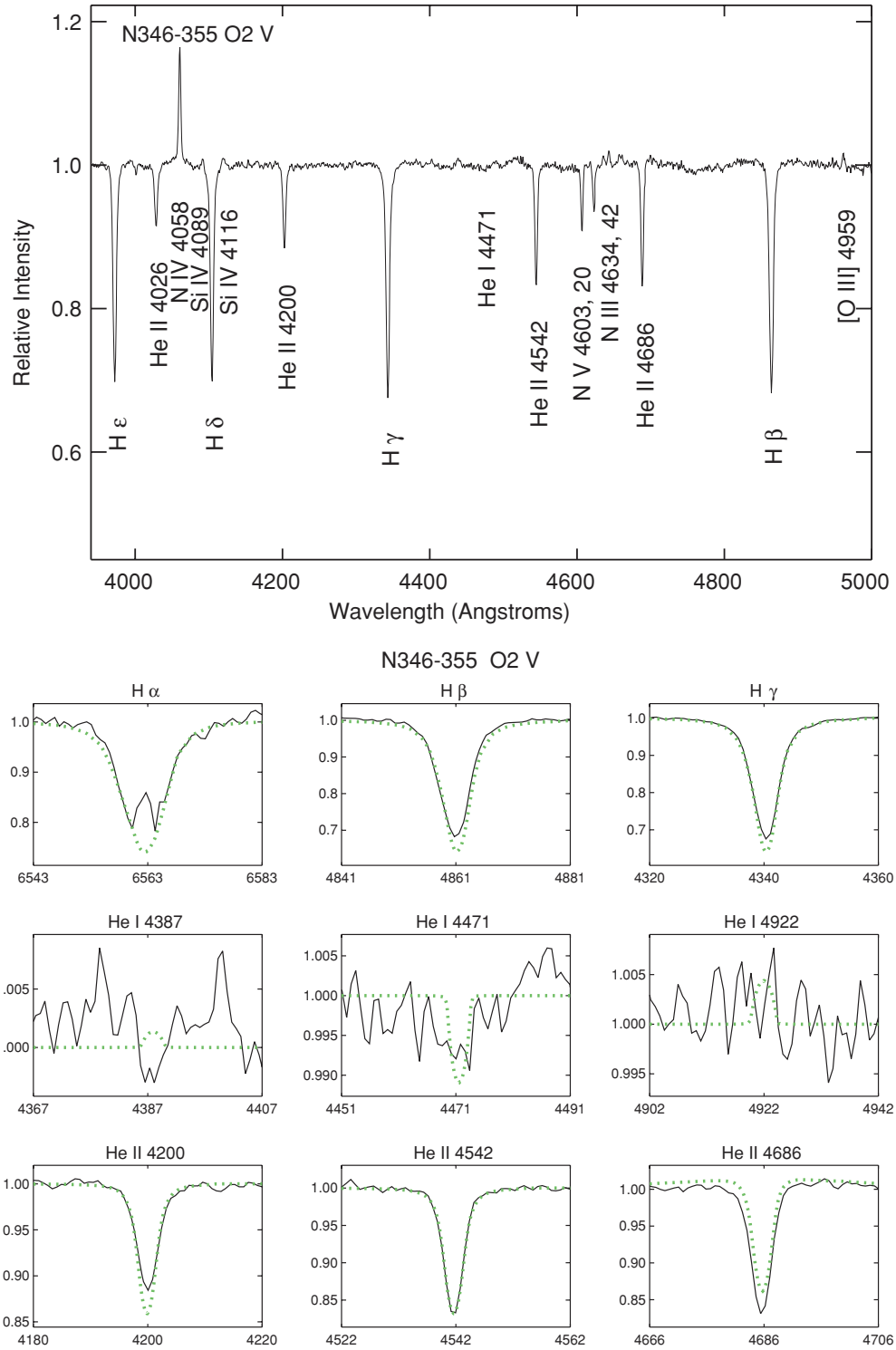

Figure 7. NGC 346−355. The upper figure shows a section of the blue spectrum of this star, with the prominent lines identified. The lower figure shows the fits (dotted) for the principal diagnostic lines.

(A color version of this figure is available in the online journal.)

The luminosity class is consistent with the absolute visual magnitude of the star, −6.71.

At our very high S/N, we actually detect weak He II lines; their EWs are 15–25 m Å, not evident in Figure 19 (upper panel) but visible in the rescaled version showing the fits in Figure 19 (lower panel). However, these provide a powerful way of constraining the effective temperature. For this star, we also used the model's Si III λ4553 and Si IV λ4089 profiles. A single effective temperature gave consistent results for He I, He II, Si III, and Si IV. We find remarkable consistency, and feel confident that the effective temperature here is determined to a precision of about 250 K (1%), unlike the typical 1000 K uncertainty for the O-type stars. Hα emission was also well fitted, but required a a value of $\beta = 2.0$. Hβ was not well fitted

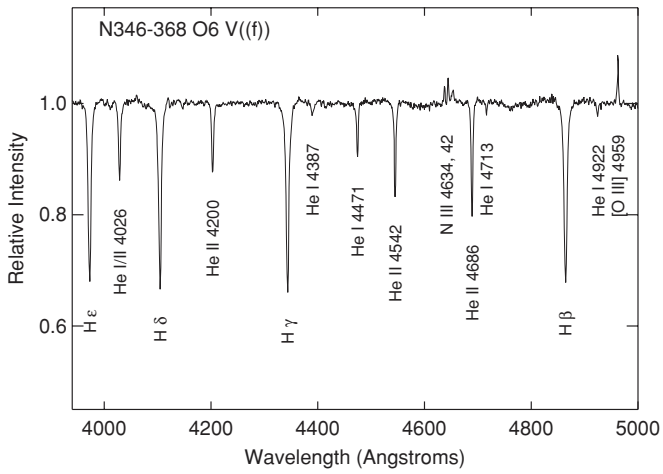

Figure 8. NGC 346−368. The figure shows a section of the blue spectrum of this star, with the prominent lines identified.

in any model with reasonable agreement in Hα. The fits are shown in Figure 19 (lower panel).

Sk−69°124. This is a late-type O supergiant (Figure 20, upper panel). We measure EWs of 830 m Å and 145 m Å, or log $W' = 0.76$. This is well beyond log $W' = 0.45$ for an O9.5 star, and so we call this O9.7. A B0 subtype is excluded on the basis that He II λ4200 is still reasonably strong (120 m Å) in our spectrum. The luminosity class is I, based upon the sharpness and strengths of the features; the O9.7 I type is also consistent with the absolute magnitude, $M_V = -6.07$. The fits are good (Figure 20, lower panel).

BI 170. This too is a late-type O supergiant (Figure 21, upper panel), although clearly not quite as late as Sk−69°124. We classify this as O9.5 I, based both on our visual comparison with the Walborn & Fitzpatrick (1990) atlas and our EW measurements for He I λ4471 (930 m Å) and He II λ4542 (310 m Å), which lead to log $W' = 0.48$. $M_V = -5.66$ is consistent with the visual appearance of the spectrum, which suggests that the star is a supergiant.

The model fits to this star were good, except for the wind lines (Figure 21, lower panel). No combination of mass-loss rate and β gave us good matches at both Hα and He II λ4686.

BI 173. This is a mid-to-late O-type giant/supergiant (Figure 22, upper panel). We measure EWs of 715 m Å and 425 m Å for He I λ4471 and He II λ4542, respectively, leading to log $W' = 0.23$, and O8.5 subtype. The luminosity class is intermediate between the giant and supergiant: N III $\lambda\lambda$4634, 42 is in emission, while He II λ4686 is weak in absorption. The absolute visual magnitude, −5.93, is closer to a supergiant than a giant. We call this star an O8.5 II(f). The fits were good, except perhaps for He II λ4686 which is slightly too strong in the model (Figure 22, lower panel). The rotation is somewhat fast, with $v \sin i = 200$ km s^{-1}.

LH 64−16. This is a very early-type O giant (Figure 23, upper panel) whose spectrum was first described as "O3 III: (f*) by Massey et al. (2000). It formed one of the prototypes of the new O2 III class introduced by Walborn et al. (2002). A subsequent analysis by Walborn et al. (2004) showed that the star was chemically enriched (both He and N) with an extremely high effective temperature, and called it an ON2 III(f*), with the "N" denoting the enhanced nitrogen abundance. The star was remodeled in Paper I. We included it in our current study because of its extreme properties and to see if we could independently reproduce its properties with our new spectra.

We aimed to obtain a much higher S/N spectrum of this star than what we used in Paper I as the He I λ4471 line was only marginally detected in that study.[11] We achieved a S/N of 1000 per 2.4 Å spectral resolution element, which confirms our detection of He I λ4471 absorption in this O2 star, again emphasizing the point made in Papers I and II that the "lack of He I" criteria originally applied to O3 stars and subsequently to the O2 class can be a S/N issue, and needs to be quantitative in order to be useful. We measure an EW of 12 m Å for He I λ4471 and an EW of 990 m Å for He II λ4542, leading to log $W' = -1.9$. (Given the much higher S/N of these data, we find that the uncertainty on the EW of the He I λ4471 line is about 5m Å, again dominated by uncertainty in the rectification.) Our fits for this star are reasonably good (Figure 23, lower panel). Note that we do not consider either He I λ4387 or He I λ4922 to have been detected; we compare the models and the spectra of these two lines in the figure purely for consistency with the other stars analyzed here. The He I λ4471 line *was* used in the fit, and the results are very similar to what we obtained in Paper I, as shown in Table 4. A very high He/H ratio was needed to obtain a reasonable fit, as we found in Paper I. There, we note that the 7× N enrichment found by Walborn et al. (2002) is consistent with any high He/H ratio (0.25–2.0), as it is simply the CNO-burning equilibrium ratio. In Table 3, note that the spectroscopic mass is only 24 $M_\odot$, while the mass inferred from the evolutionary tracks is much higher, 74 $M_\odot$. In accord with Paper I, we suggest that this star is the result of binary evolution other than a normal evolutionary process.

Sk−67°166, HD 269698. This star has been previously called an O4 If+ star by Walborn (1977), a classification with which we concur (Figure 24, upper panel): we measure EWs of 115 m Å and 670 m Å for He I λ4471 and He II λ4542, respectively, leading to log $W' = -0.76$. N III $\lambda\lambda$4638, 42 and He II λ4686 are strong in emission, leaving no ambiguity about the luminosity class being a supergiant, in agreement with $M_V = -6.5$.

Our fits for this star were relatively good (Figure 24, lower panel), although we had to increase the He/H ratio to 0.20. The He II λ4542 model line is weaker than that observed, although the He II λ4200 line is in good agreement. For He I, we detected only the λ4471 line, but included the λ4387 and λ4922 lines in the figure for consistency. The star had been previously modeled by Puls et al. (1996) and Mokiem et al. (2007). Our parameters are very similar to those derived by the latter study, which also used the modern version of FASTWIND.

BI 192. Visually, this is a mid-to-late O giant/supergiant (Figure 25, upper panel). We measure EWs of 800 m Å and 300 m Å for He I λ4471 and He II λ4542, respectively, leading to log $W' = 0.42$, an O9 subtype. The absolute visual magnitude is −5.03, consistent with the star being a giant, as is spectrally indicated by the relative strengths of the Si IV and He I features. The fits are all quite good (Figure 25, lower panel).

BI 208. At first glance, we would assign an O6–O6.5 subtype to this star, along with a luminosity class of V((f)) as He I λ4471 is marginally weaker than He II λ4542, N III $\lambda\lambda$4638, 42 is in emission but He II λ4686 is strong in absorption (Figure 26, upper panel). Our EW measurements of 510 m Å and 830 m Å for He I λ4471 and He II λ4542, respectively, leading

[11] Note that the EW of He I λ4471 was incorrectly reported in Paper II as 100 m Å, rather than ∼ 10 m Å. We have compared our new spectra with those used in Paper I and they are quite similar; the problem was a typographical error in Table 7 of Paper II and the subsequent use of this number to report an erroneous log W' in Paper II.

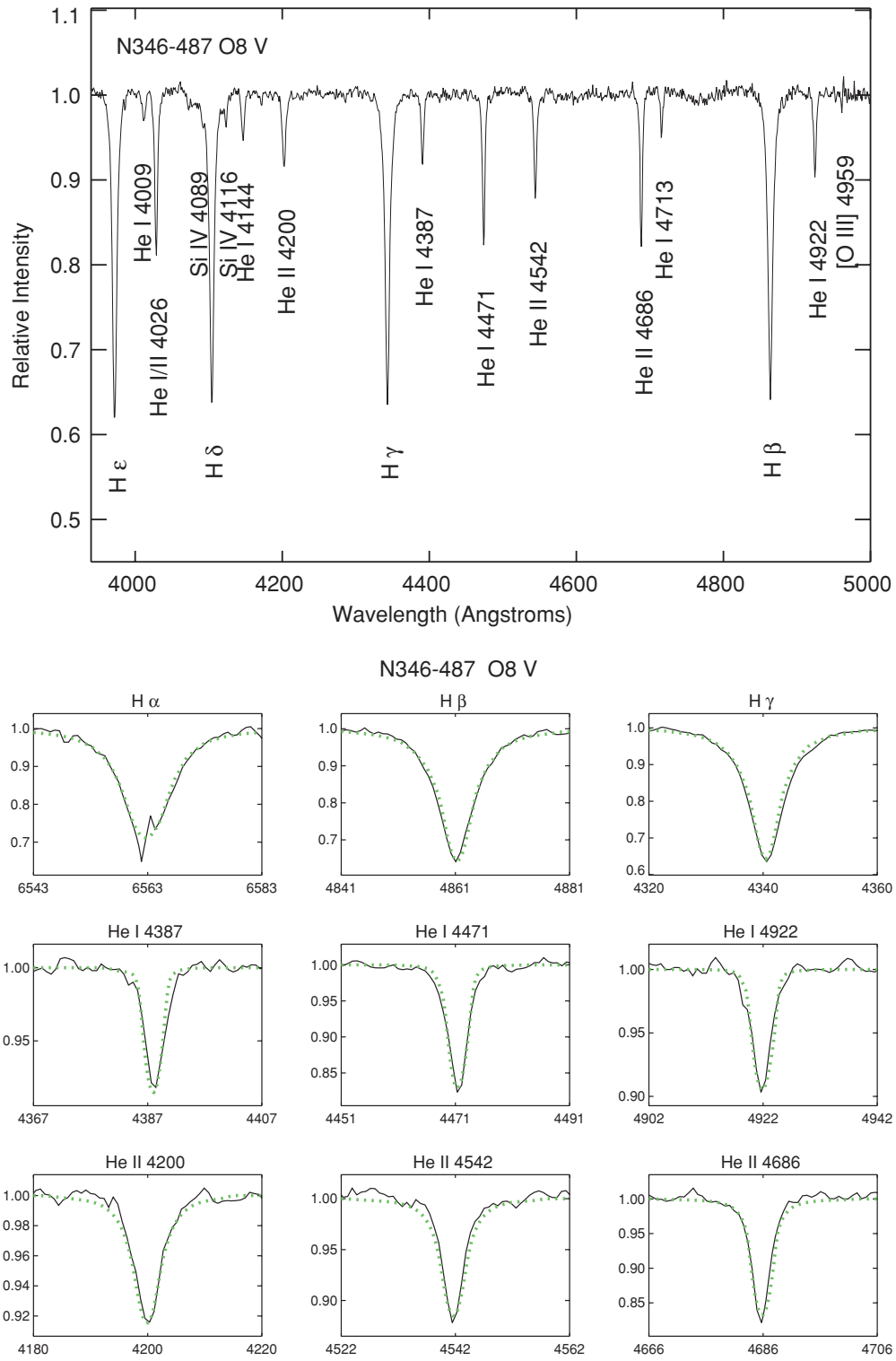

Figure 9. NGC 346−487. The upper figure shows a section of the blue spectrum of this star, with the prominent lines identified. The lower figure shows the fits (dotted) for the principal diagnostic lines.

(A color version of this figure is available in the online journal.)

to $\log W' = -0.21$ make it just marginally an O6 subtype rather than an O6.5. The absolute visual magnitude of −4.87 is consistent with the star being a dwarf, and so we classify the star as O6 V((f)).

The fits for this star were quite good (Figure 26, lower panel). The terminal velocity measured by Prinja & Crowther (1998) is listed as uncertain; it is quite small compared to the expected $2.6v_{\rm esc}$ (Table 2). We ran additional models using a more likely value, 2000 km s^{-1}, to see what effect this would have on our modeling of this star, and the differences were minor. A slightly higher mass-loss rate was needed (0.5 rather than 0.3 in units of 10^{-6} $M_\odot$ yr^{-1}) but the fits were otherwise similar. The only other peculiarity we note is a slightly larger than the usual discrepancy (60 km s^{-1}) between the blue and red radial

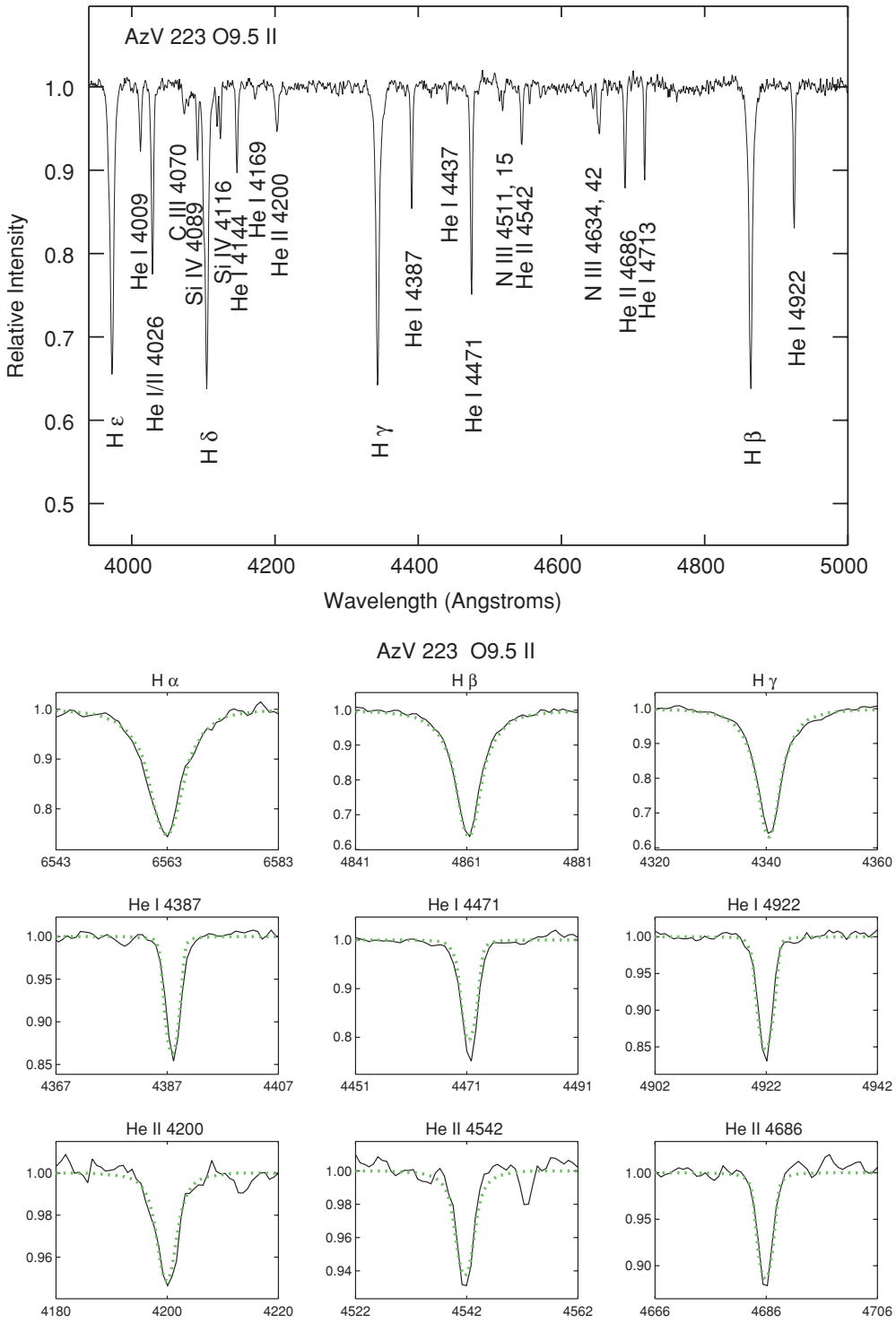

Figure 10. AzV 223. The upper figure shows a section of the blue spectrum of this star, with the prominent lines identified. The lower figure shows the fits (dotted) for the principal diagnostic lines.

(A color version of this figure is available in the online journal.)

velocities. In the absence of any other evidence of binarity, we retain this star in our analysis.

4. RESULTS AND DISCUSSION

4.1. Comparisons with Other Model Results

We have attempted to model the spectra of 26 Magellanic Cloud O and early B stars, 14 in the SMC and 12 in the LMC. We have succeeded in 18 cases (69%), with the rest likely being spectroscopic binaries or showing circumstellar features that rendered good fits impossible.

How do our results compare to those of others? In Paper II, we considered our effective temperature scale (effective temperature as a function of spectral type) in comparison with those determined by others, finding that our FASTWIND-derived SMC scale was warmer by several thousand degrees than the effective temperatures determined for several NGC 346 stars by Bouret et al. (2003) using TLUSTY and CMFGEN.

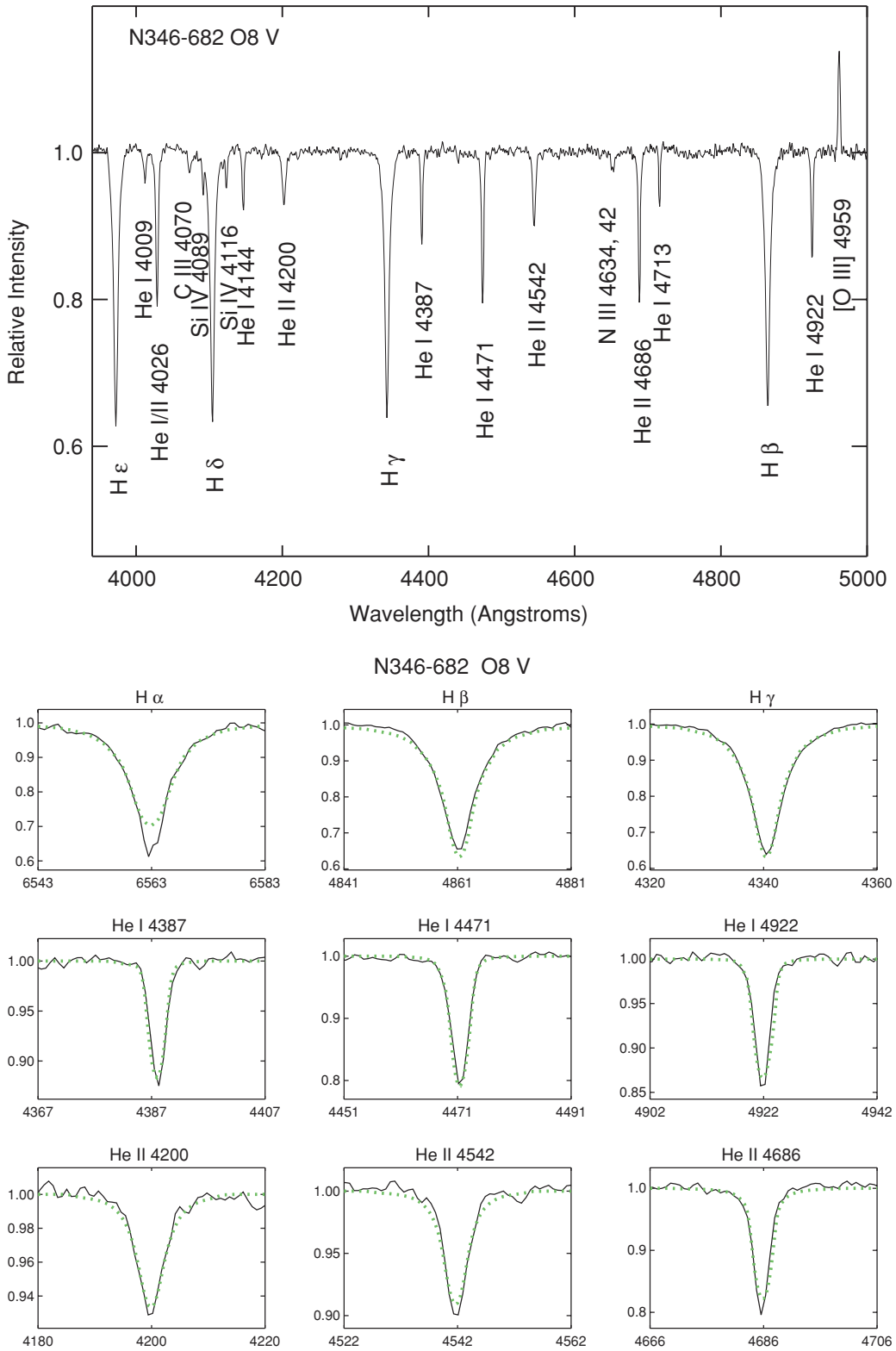

Figure 11. NGC 346−682. The upper figure shows a section of the blue spectrum of this star, with the prominent lines identified. The lower figure shows the fits (dotted) for the principal diagnostic lines.

(A color version of this figure is available in the online journal.)

However, very few stars were in common among various studies at the time, making it difficult to compare the results directly. The current study was largely motivated by this frustration.

In Table 4, we compare the model results for the stars analyzed in this study with those by others, and in Table 5, we extend this to other stars in common in Papers I and II with others. Several trends emerge from this comparison. First, we find that the

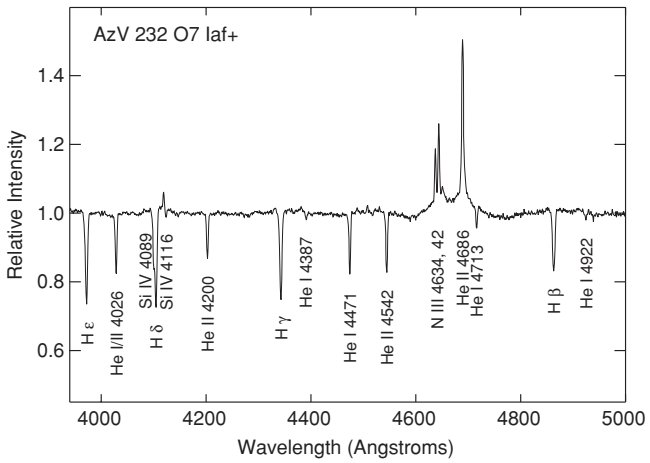

Figure 12. AzV 232. The figure shows a section of the blue spectrum of this star, with the prominent lines identified.

automatic fitting procedure with FASTWIND used by Mokiem et al. (2006, 2007) produced effective temperatures that were 1100 K warmer (on average)[12] for the 11 stars in common for which we found an acceptable fit. We attribute these differences to the different weights given to fitting various lines: we relied heavily upon He I λ4387 and (in the nonsupergiants) He I λ4471 in determining our best fits.

More significant perhaps is the fact that the automatic fitting procedure of Mokiem et al. (2006, 2007) always finds *some* fit that is "best," resulting in their deriving physical properties of stars that we find to be clearly composite. For example, in Paper I, AzV 372 was found to have He I lines significantly broader than the He II lines as well as a radial velocity shift between the He I and He II lines. We expect from studies of Galactic O stars that at least 36% are spectroscopic binaries (Garmany et al. 1980), with the true percentage of composites probably higher. Thus it would be remarkable in an analysis of a large sample of O-type stars to always come up with an acceptable fit (see discussion following de Koter 2008). The LMC sample (Mokiem et al. 2007) was "prefiltered" to avoid stars that showed radial velocity variations in their data, but no such selection was made for their SMC sample, and in neither case was the goodness of fits used other than to assign uncertainties to the physical properties. (We are indebted to C. Evans for clarifying this situation for us.) In any event, this problem could be avoided in future work by providing some objective "goodness of fit" criteria that distinguish cases where the "best" fit is not good, as per the general discussion in Press et al. (1992).

There are fewer stars (seven with good fits) in common with our studies and the TLUSTY analysis of Bouret et al. (2003) and Heap et al. (2006), but here we find a much larger range of differences (from −3000 K to +3500 K), with a median difference of 1000 K. Thus the differences we saw in Paper II between our temperature calibration and the results for their stars were not due to a systematic effect between the different modeling techniques, but rather due to issues with particular stars. For example, as we noted above, Heap et al. (2006) retained the star NGC 346−368 in their determination of their effective temperature scale, even though they (and we) concluded that it is a binary. In some cases, the adopted spectral types do not match: for NGC 346−368, they adopted the O4-5 V ((f)) type of Walborn et al. (2000), while we find a type of O6 V here. This type mismatch could be in part caused by the lack of nebular subtraction in the Walborn et al. (2000) data, and in other cases could be the result of improper sky subtraction. As noted in Paper II, the Anglo-Australian Telescope (AAT) Echelle spectra used by Walborn et al. (2000) for spectral classification were incorrectly corrected for moonlight contamination; they described a procedure that removed the solar line absorption spectrum, but would have left the moonlight continuum contribution contaminating the spectrum. C. Evans (2005, private communication) reports that he was subsequently able to correct the spectra for most stars used in the analysis by Bouret et al. (2003) and Heap et al. (2006), but that there were insufficient sky pixels for sky subtraction for NGC 346−368 and NGC 346−487. Yet these stars were included in their analysis. How large a difference did this make in practice? We give a comparison for NGC346−487 in Figure 27. The AAT lines are weaker, as would be expected from uncorrected night sky contamination. The differences in EWs are significant: in the AAT data, we measure 240 m Å for He II λ4200, 270 m Å for He I λ4387, and 300 m Å for He II λ4542, while in our own data we measure 530 m Å, 350 m Å, and 615 m Å, respectively, which are factors of 2.2, 1.3, and 2.1 higher. Thus, modeling involving these lines would invariably lead to discordant results compared with ours. Clearly, He I λ4471 would not provide many constraints in the AAT data. Recall that Bouret et al. (2003) were unable to obtain a good fit to the optical spectrum of this star and had to primarily rely on their UV data. We derive very different results for this star, with our measurement 3000 K hotter and a log g that is 0.2 dex higher, as shown in Table 4.

What about the other stars? We find the other star with no sky subtraction in their data, NGC 346−368, to be a binary. For NGC 346−324, our results are in very good agreement, with our temperature 500 K hotter. For that star, we measure EWs of 200 m Å and 760 m Å for He I λ4471 and He II λ4542, respectively, compared with 250 m Å and 760 m Å in our own data, in reasonable agreement. The difference is in the opposite sense than expected, though, in that our slightly stronger line should lead to a slightly cooler temperature, everything else being equal. For NGC 346−355, we are unable to measure He I in their spectra; we detect this line at the 50 m Å level, thanks to our much higher S/Ns. For He II λ4542, we measure an EW of 685 m Å in their data, while in ours we measure 720 m Å, again in substantial agreement. The large difference in the derived effective temperature (our 49,500 K value versus their 52,500 K value) is presumably due to the fact that we were able to detect He I, which constrained the effective temperature. Bouret et al. (2003) did also model UV data, which provided additional constraints; we plan such an extension to our work in the future, as discussed further below.

4.2. Effective Temperature Scale

In Paper II, we presented a revised effective temperature scale for O-type stars, based upon our analysis with FASTWIND of a sample of O stars in the SMC and LMC, as well as the study by Repolust et al. (2004) of Galactic stars. We presented in a tabular form our revised scale for the SMC supergiants, SMC giants and dwarfs (which appeared to be indistinguishable), Galactic supergiants, and Galactic giants and dwarfs. Unsurprisingly, we found a substantial difference between the SMC and Galactic

[12] This is the *median* difference; for some stars, the differences are even greater, such as for Sk−70°69, where Mokiem et al. (2007) find an effective temperature that is 2700 K higher as well as a higher surface gravity.

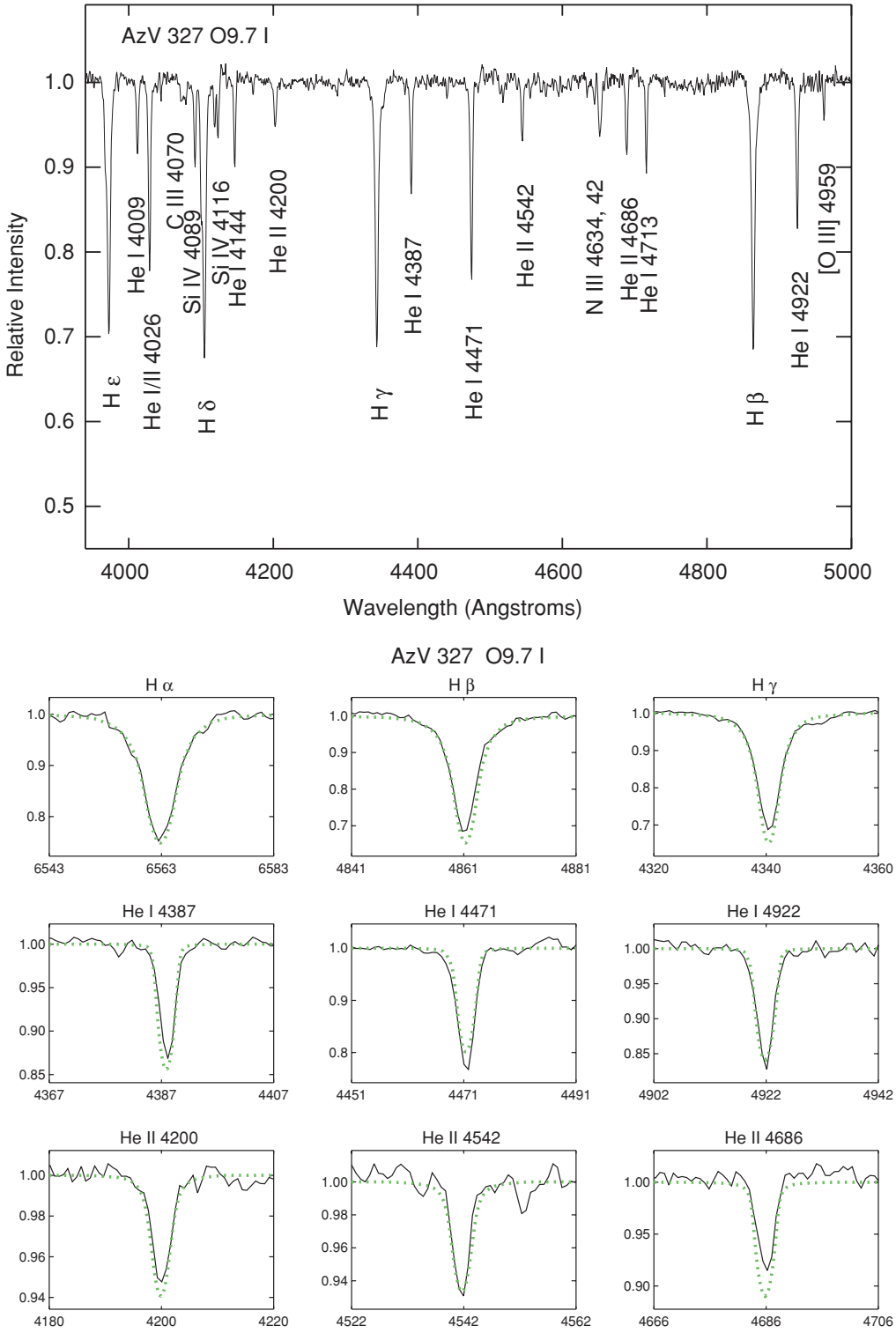

Figure 13. AzV 327. The upper figure shows a section of the blue spectrum of this star, with the prominent lines identified. The lower figure shows the fits (dotted) for the principal diagnostic lines.

(A color version of this figure is available in the online journal.)

effective temperature calibrations, with the SMC scale significantly hotter (3000–4000 K) for the early O's, with negligible differences by B0. This is in accord with the expected effects of wind blanketing and line blanketing, which will be less significant at lower metallicities. The data were too scant to determine a scale for the LMC stars, although our data showed that the temperatures for LMC stars were intermediate between those for SMC and Milky Way stars, as would be expected from their metallicity.

With the large sample of stars, we revisit this issue here. In Figure 28 (upper panel), we now show all of the SMC data from Papers I, II, and the present work, along with the SMC effective

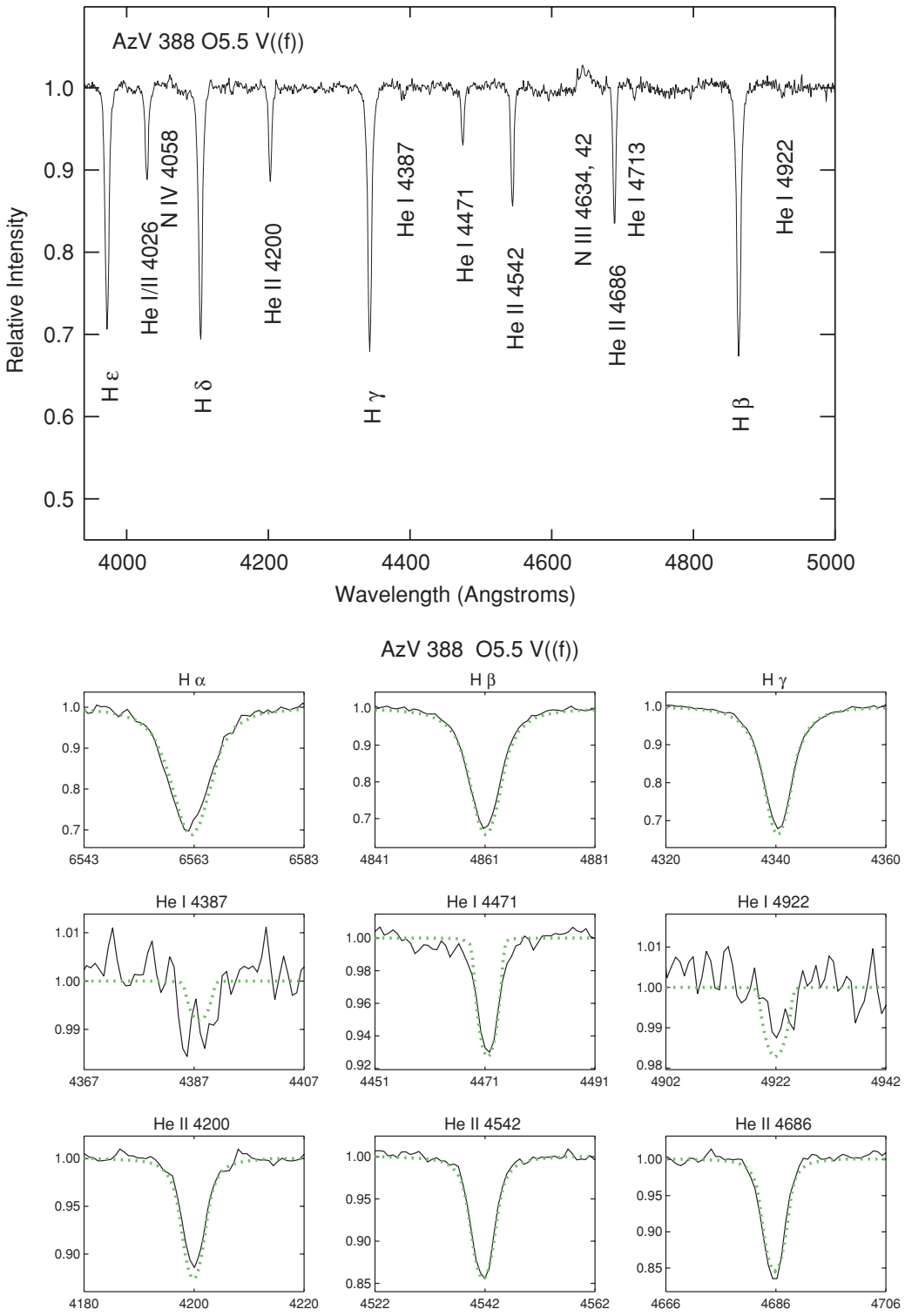

Figure 14. AzV 388. The upper figure shows a section of the blue spectrum of this star, with the prominent lines identified. The lower figure shows the fits (dotted) for the principal diagnostic lines.

(A color version of this figure is available in the online journal.)

temperature calibration. Filled symbols show data from the present paper in order to demonstrate how the current study has improved our coverage of spectral types. Dwarfs are indicated by circles, giants by squares, and supergiants by triangles. The proposed dwarf and giant effective temperature scale is shown by a solid line and that of the supergiants by a dashed line.

We see that the new data are in reasonable accord with the adopted relationship. If anything, the dwarf and giant sequence may be a little hotter than it should be for the earlier types. Note that, even with the new data, there are no constraints on the supergiant sequence for stars earlier than O5 I.

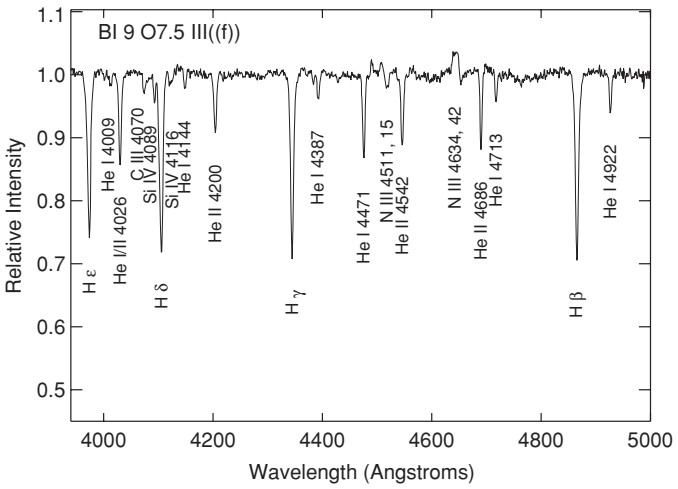

Figure 15. BI 9. The figure shows a section of the blue spectrum of this star, with the prominent lines identified.

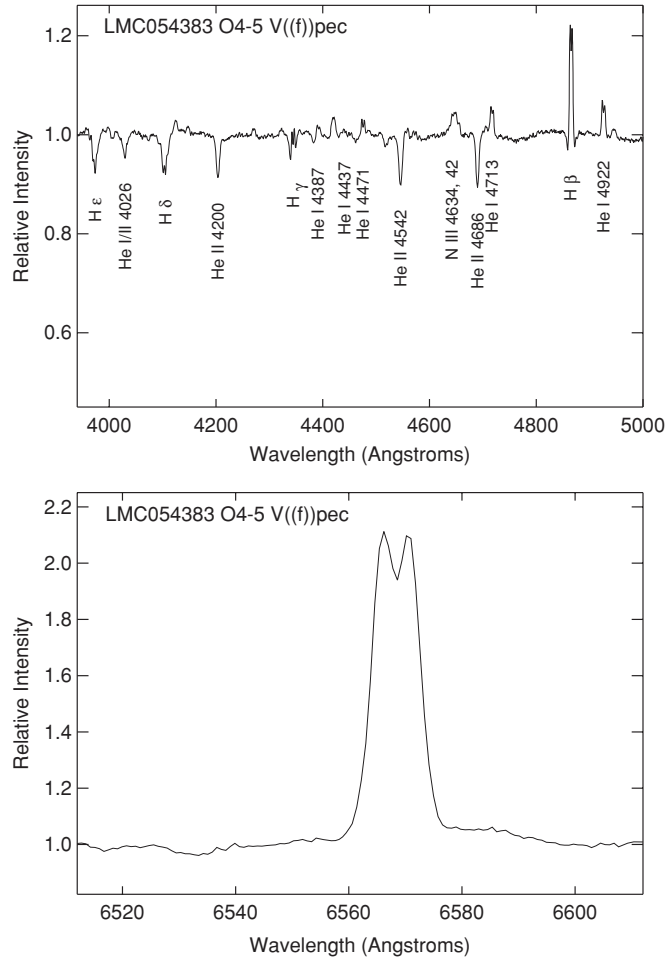

Figure 16. LMC 054383. The upper figure shows a section of the blue spectrum of this star, with the prominent lines identified. The lower figure shows the Hα profile.

What of the LMC stars? In Figure 28 (lower panel), we now add these stars to the mix using red to distinguish them from the SMC stars, but otherwise retaining the same symbols. For simplicity, we have excluded the O2–3.5 stars of uncertain types from Papers I and II. We see that there is little to no difference

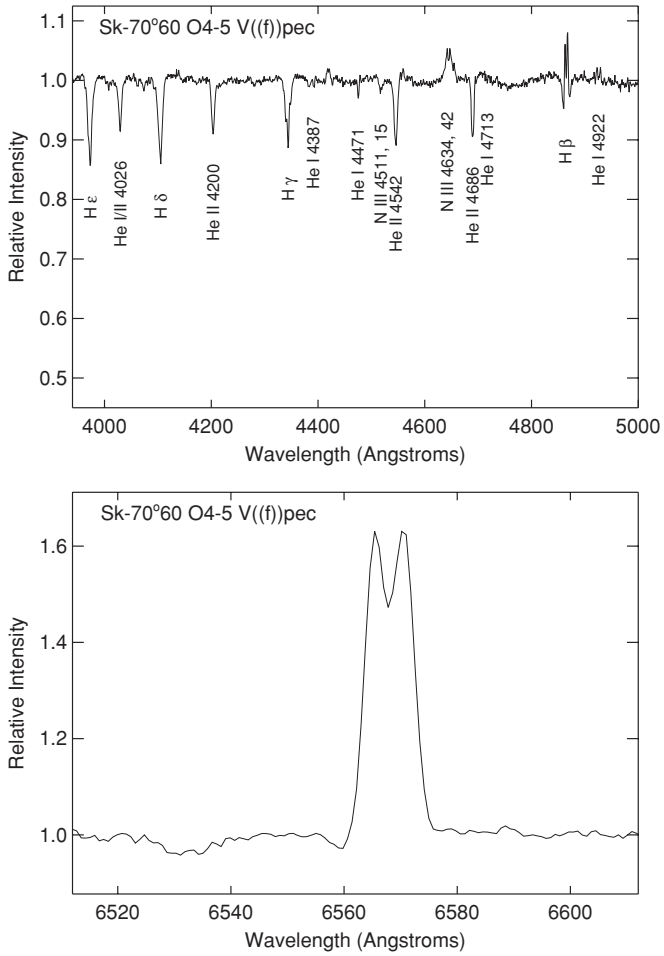

Figure 17. Sk−70°60. The upper figure shows a section of the blue spectrum of this star, with the prominent lines identified. The lower figure shows the Hα profile.

between LMC and SMC stars by the late O/early B types (even, surprisingly, for supergiants), but that for earlier types the LMC stars *are* cooler than their SMC counterparts. Again, this is what is expected. We also see with the new data that giants may indeed be intermediate in effective temperature between dwarfs and supergiants, at least for the earlier types.

What is needed to further refine these relationships? For the LMC stars, we need analysis of more mid- and late-type O dwarfs, and mid-type supergiants. For the SMC, the analysis of early-type supergiants would be useful. For now, we retain the effective temperature scale laid out in Table 9 of Paper II.

4.3. The Mass Discrepancy Revisited

Groenewegen et al. (1989) were the first to describe the "mass discrepancy," which was subsequently studied extensively by Herrero et al. (1992). The "spectroscopic mass" follows directly from the results of modeling the spectra, with $M_{\rm spect} = (g_{\rm true}/g_{\odot})R^2$ (where the mass and the radius are expressed in solar units). However, the effective temperature and luminosity from the modeling also imply a mass, which we call the "evolutionary mass" ($M_{\rm evol}$), from the evolutionary tracks. The mass discrepancy refers to the systematic difference between these two. Early studies found that the spectroscopic mass was systematically less than the evolutionary mass by as

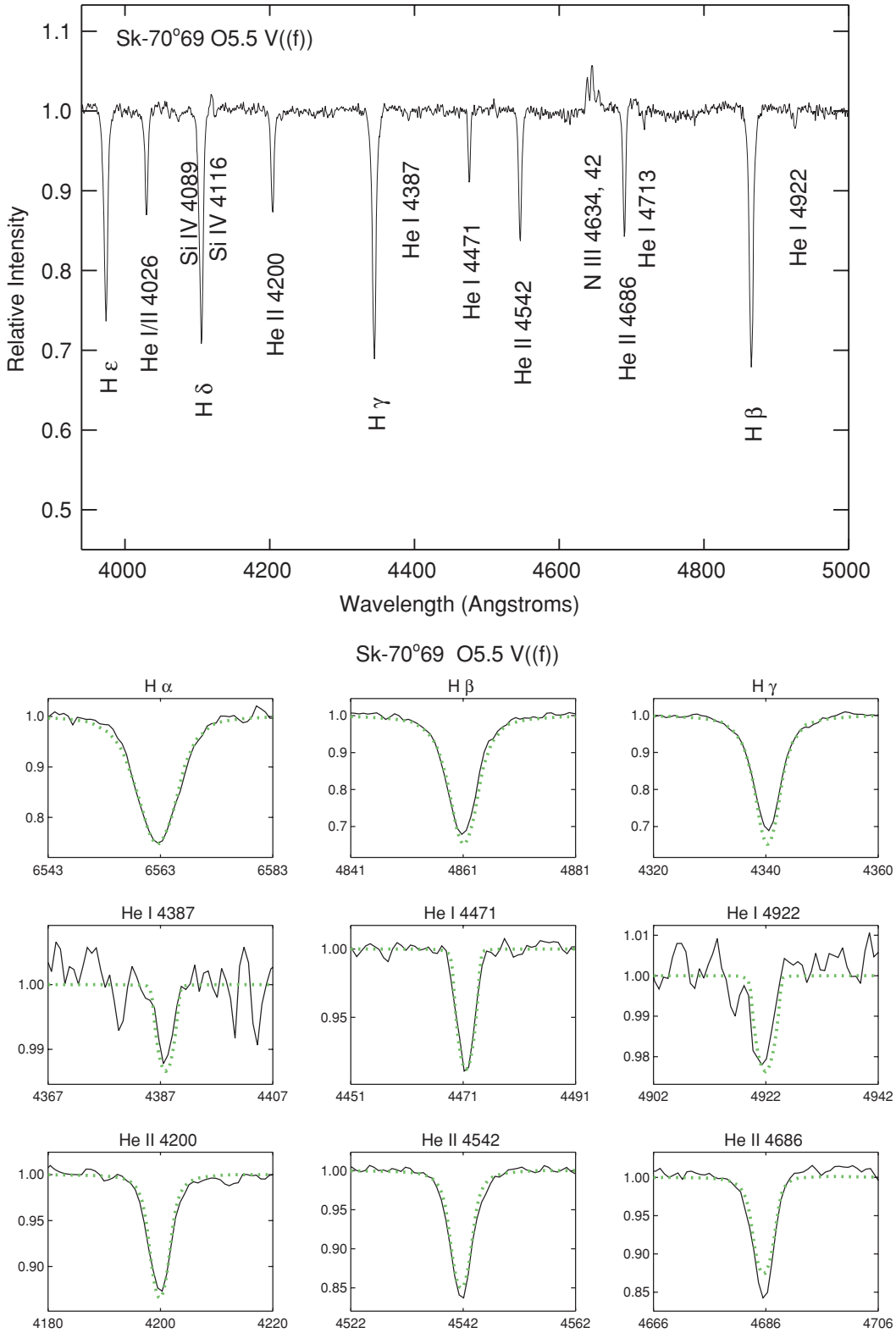

Figure 18. Sk−70°69. The upper figure shows a section of the blue spectrum of this star, with the prominent lines identified. The lower figure shows the fits (dotted) for the principal diagnostic lines.

(A color version of this figure is available in the online journal.)

much as a factor of 2 for supergiants. Improvements in the stellar atmosphere models have decreased or eliminated the size of the discrepancy for Galactic stars (Herrero 2003; Repolust et al. 2004; Mokiem et al. 2005). As we discussed in Paper II, the expected reason is twofold: the new atmosphere models include line blanketing and thus result in lower effective temperatures,

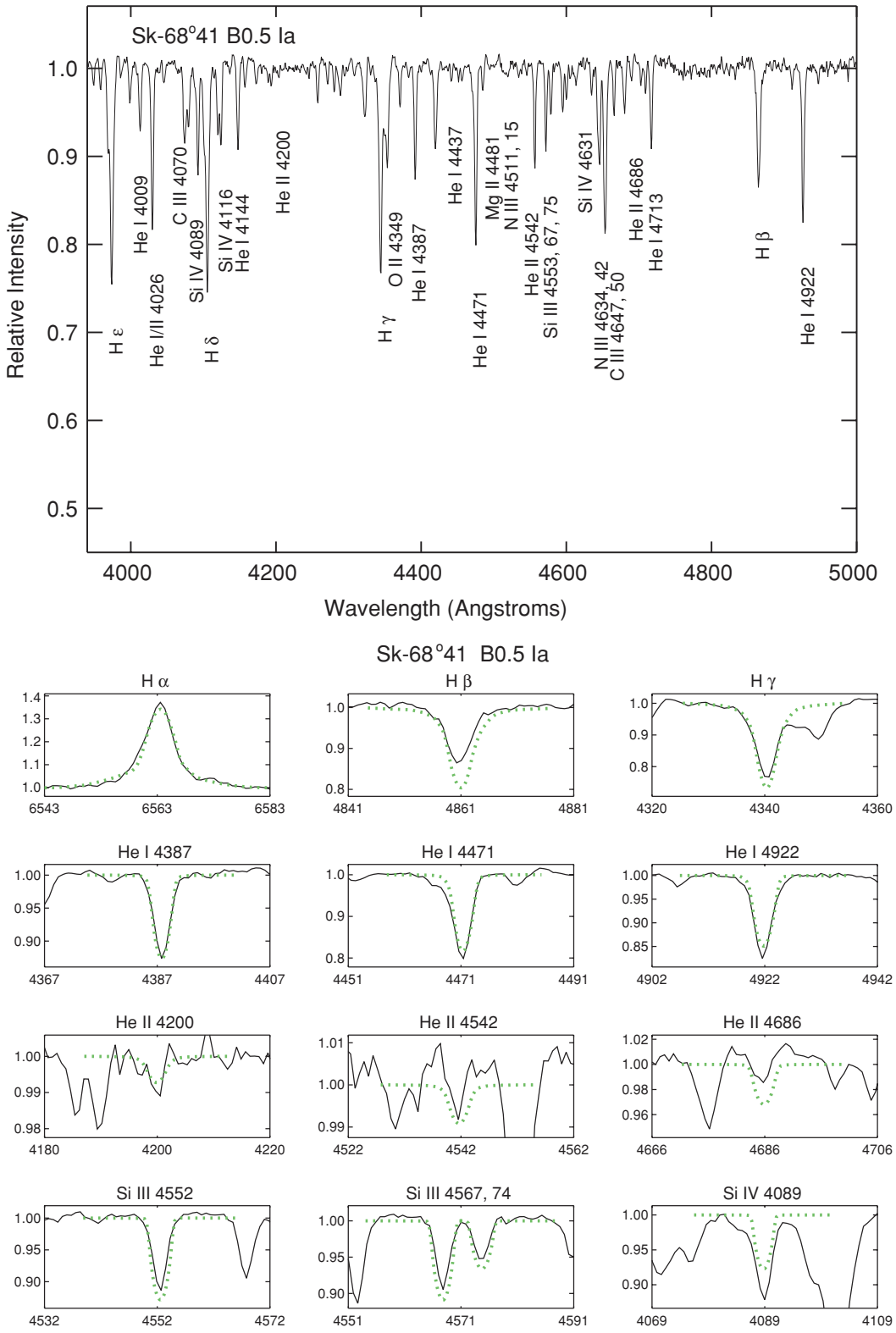

Figure 19. Sk−68°41. The upper figure shows a section of the blue spectrum of this star, with the prominent lines identified. The lower figure shows the fits (dotted) for the principal diagnostic lines.

(A color version of this figure is available in the online journal.)

decreasing the inferred luminosities, and hence the deduced evolutionary mass will be less. In addition, the new models result in larger photospheric radiation pressure, so a higher surface gravity is needed to reproduce the Stark-broadened wings of the Balmer lines. (To some extent, however, this is offset by the fact that the cooler temperatures require a lower surface gravity to fit the Balmer lines; see Repolust et al. 2004.) However, in Paper II, we found that there was still a mass discrepancy for the hottest O stars in the Magellanic Clouds. Here, we revisit the issue.

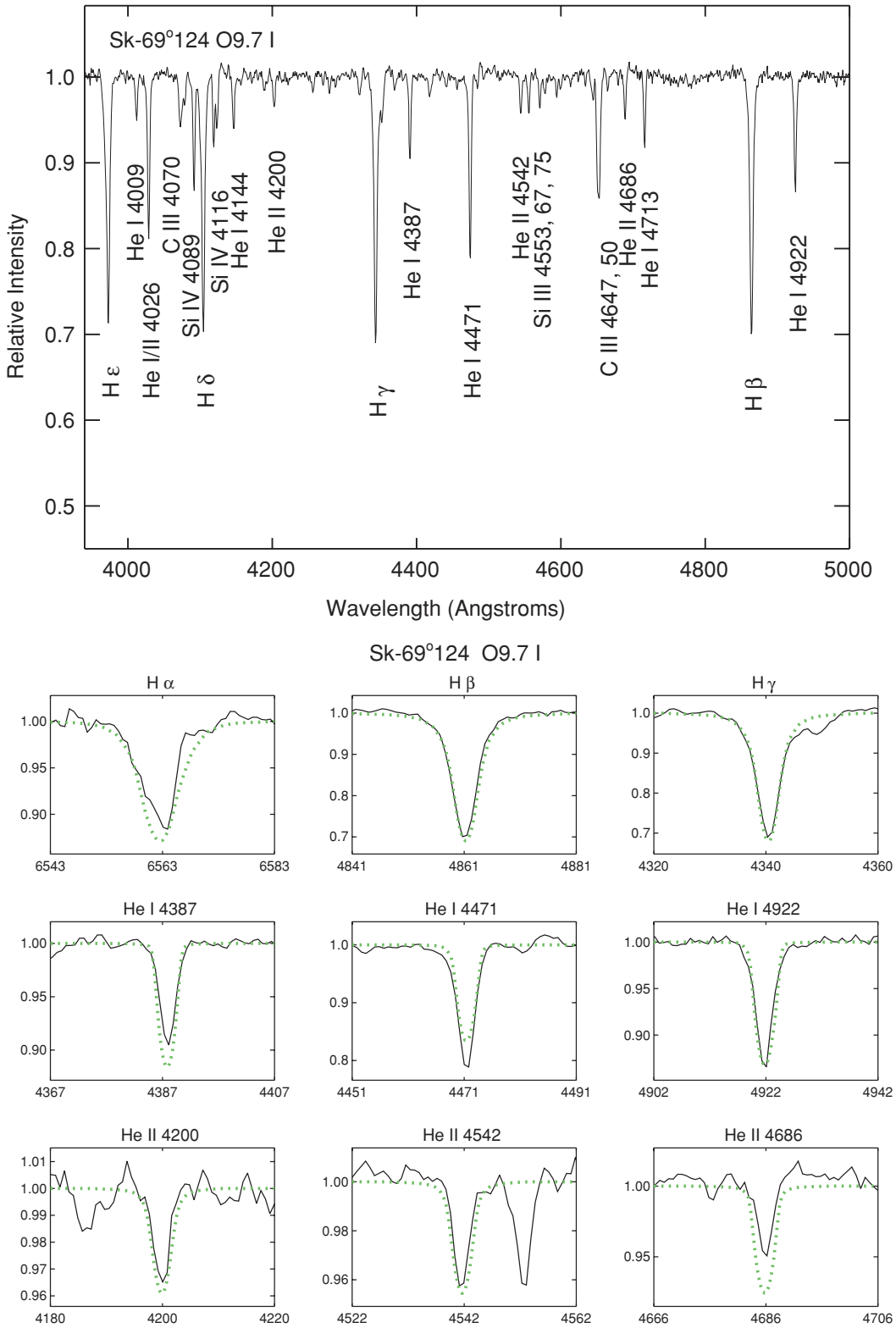

Figure 20. Sk−69°124. The upper figure shows a section of the blue spectrum of this star, with the prominent lines identified. The lower figure shows the fits (dotted) for the principal diagnostic lines.

(A color version of this figure is available in the online journal.)

In Figure 29, we plot the evolutionary mass versus the spectroscopic mass. Although many points cluster along the 1:1 line, there are still a substantial number of points significantly above the line. The error bars are based on the same assumptions as in Paper II. It is clear that the mass discrepancy is still very much with us, at least in the Magellanic Clouds. We have

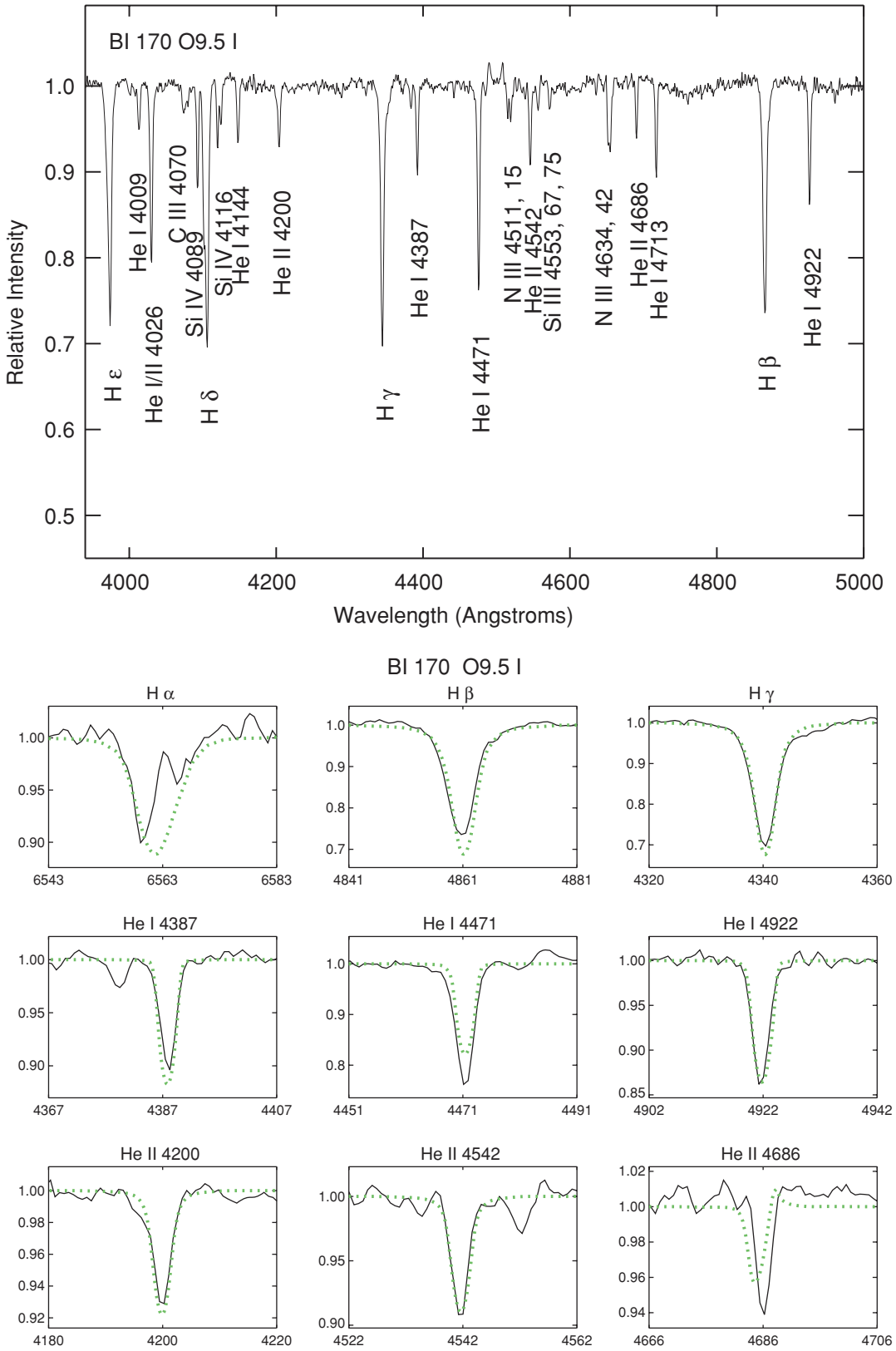

Figure 21. BI 170. The upper figure shows a section of the blue spectrum of this star, with the prominent lines identified. The lower figure shows the fits (dotted) for the principal diagnostic lines.

(A color version of this figure is available in the online journal.)

used the same symbols as before: circles are dwarfs, squares are giants, and triangles are supergiants. Filled symbols denote the new results here, while open symbols come from Papers I and II. (We have included stars of uncertain spectral types but

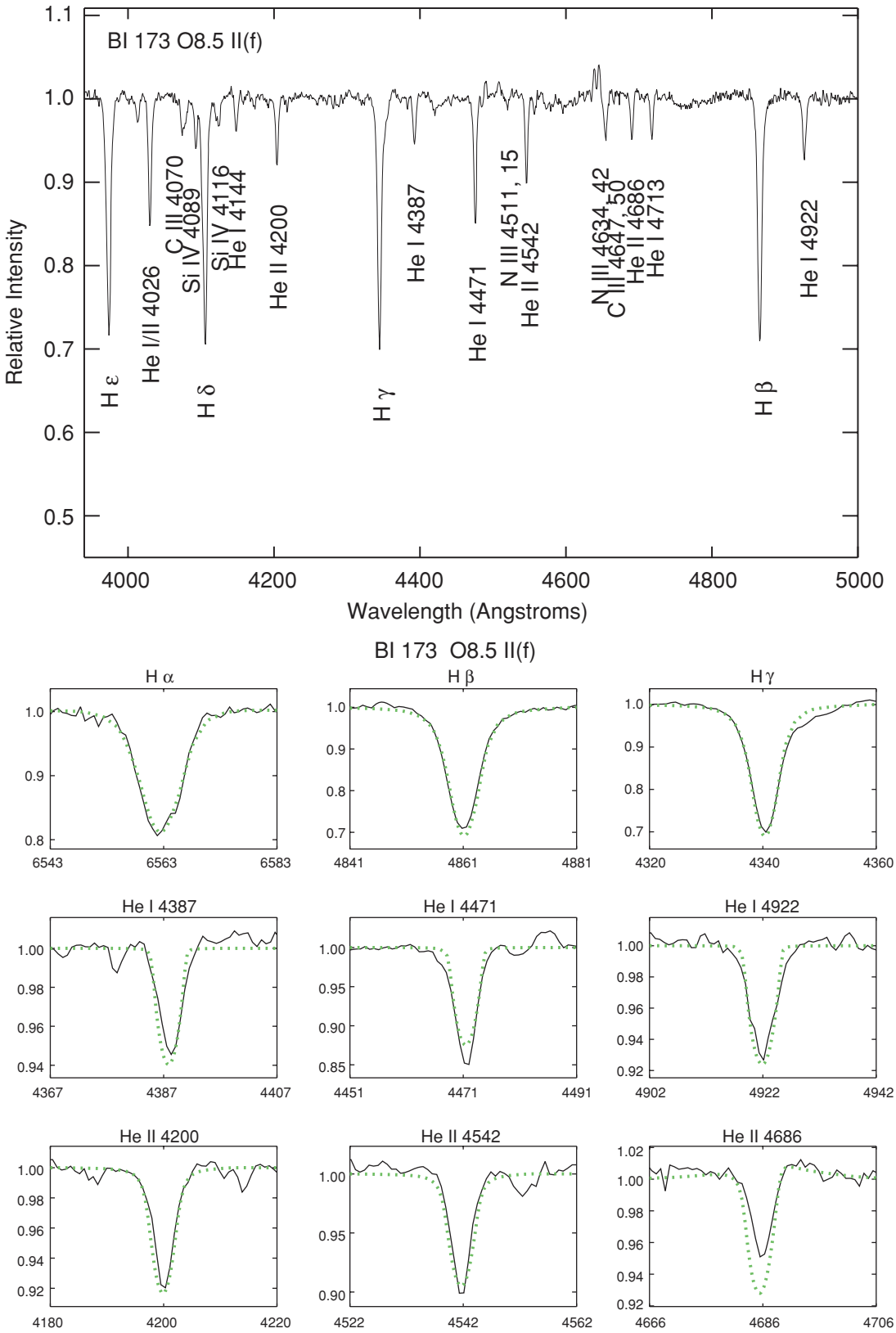

Figure 22. BI 173. The upper figure shows a section of the blue spectrum of this star, with the prominent lines identified. The lower figure shows the fits (dotted) for the principal diagnostic lines.

(A color version of this figure is available in the online journal.)

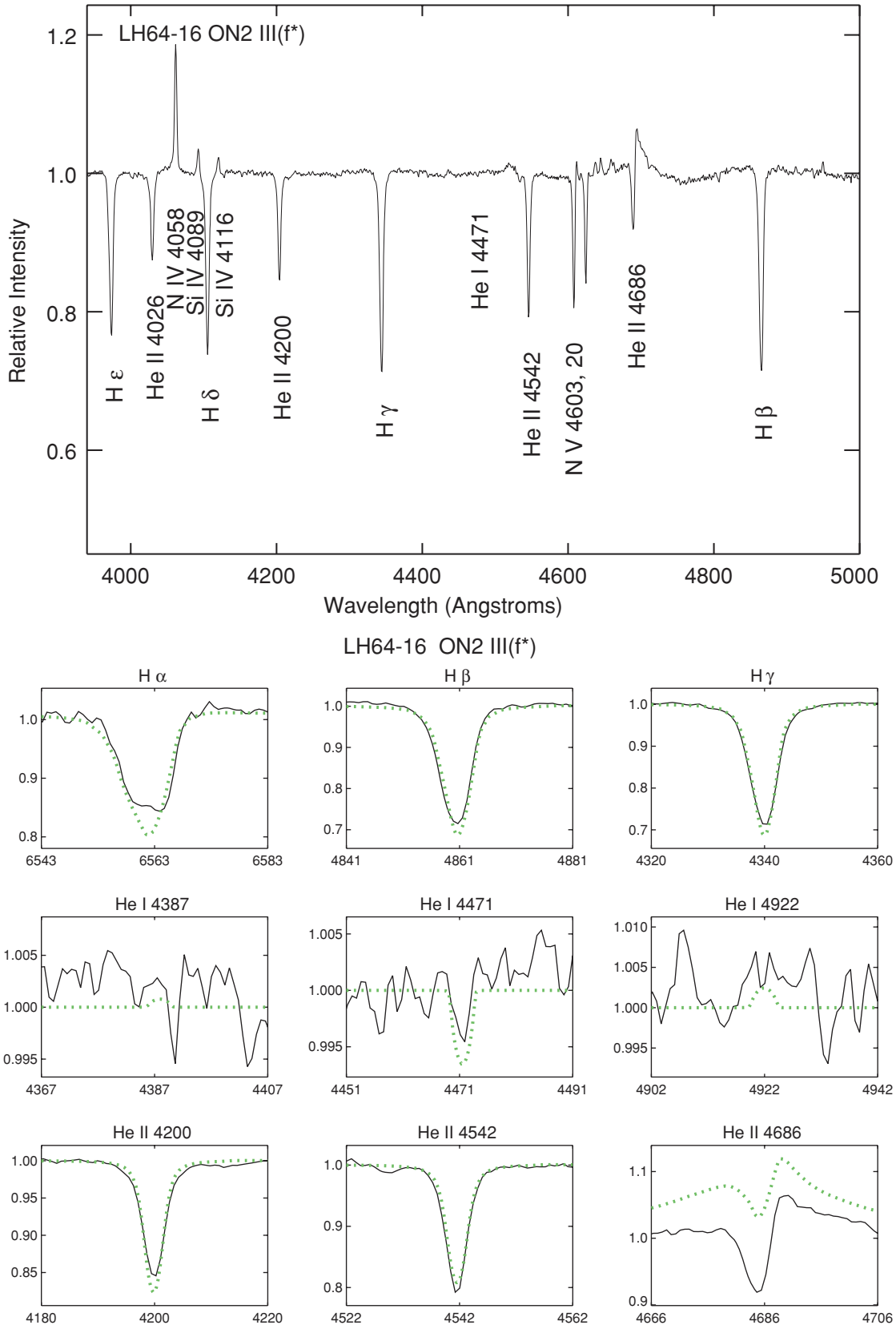

Figure 23. LH 64−16. The upper figure shows a section of the blue spectrum of this star, with the prominent lines identified. The lower figure shows the fits (dotted) for the principal diagnostic lines.

(A color version of this figure is available in the online journal.)

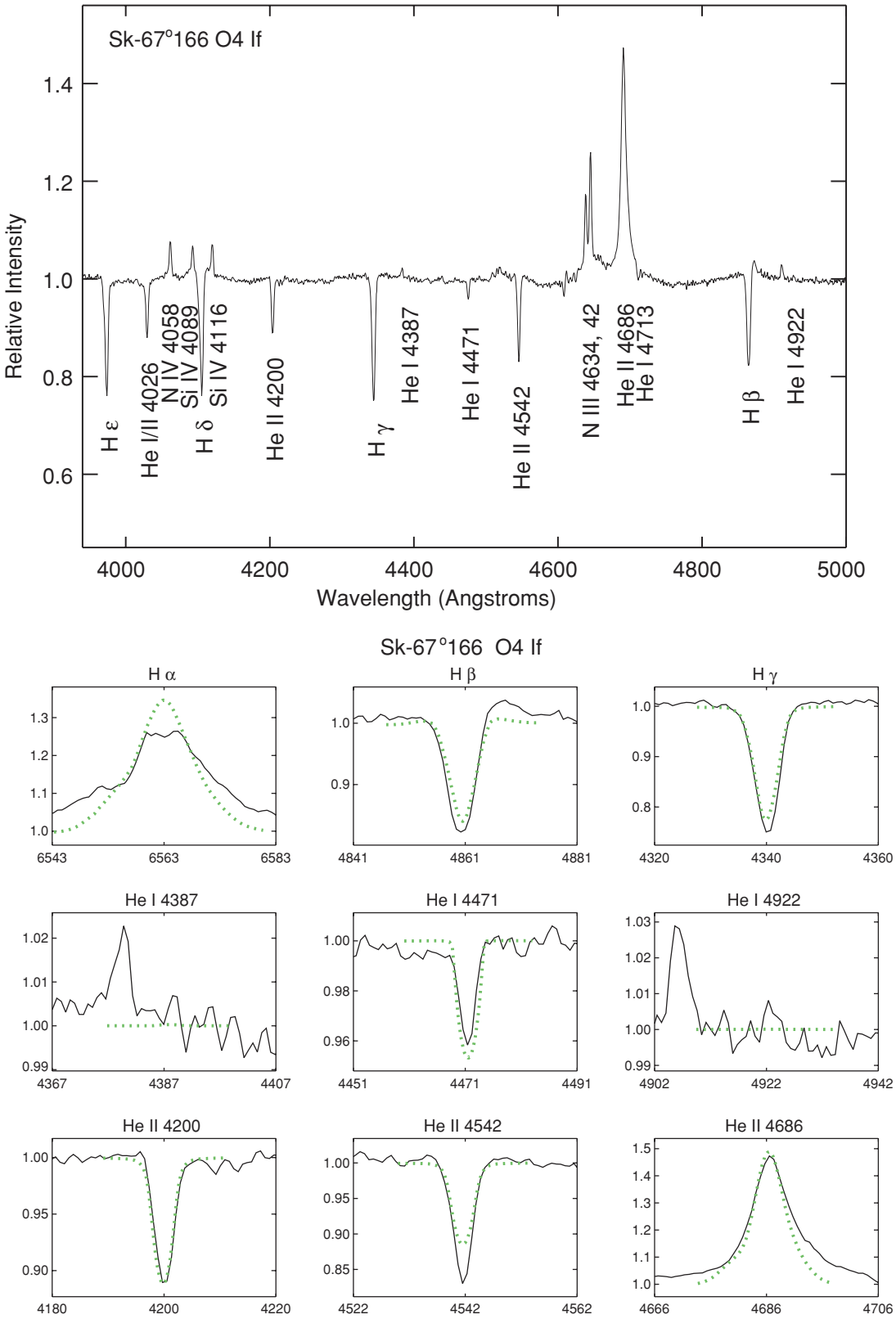

Figure 24. Sk−67°166. The upper figure shows a section of the blue spectrum of this star, with the prominent lines identified. The lower figure shows the fits (dotted) for the principal diagnostic lines.

(A color version of this figure is available in the online journal.)

excluded any stars for which we derived only a lower limit to their effective temperatures.) In Paper II, we suggested that the stars with a significant mass discrepancy were those with the highest effective temperatures, $T_{\rm eff} > 45{,}000$ K. Here, we

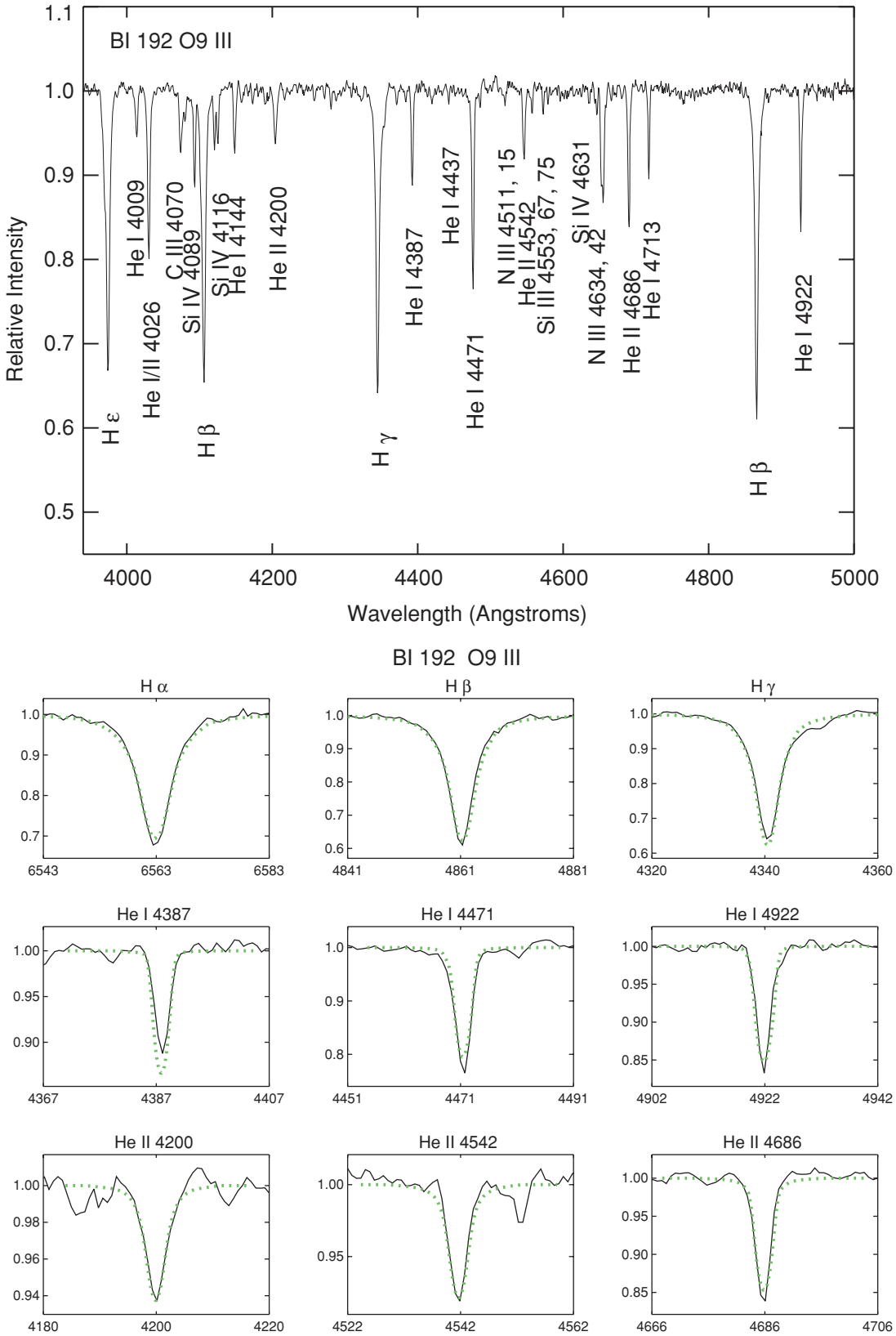

Figure 25. BI 192. The upper figure shows a section of the blue spectrum of this star, with the prominent lines identified. The lower figure shows the fits (dotted) for the principal diagnostic lines.

(A color version of this figure is available in the online journal.)

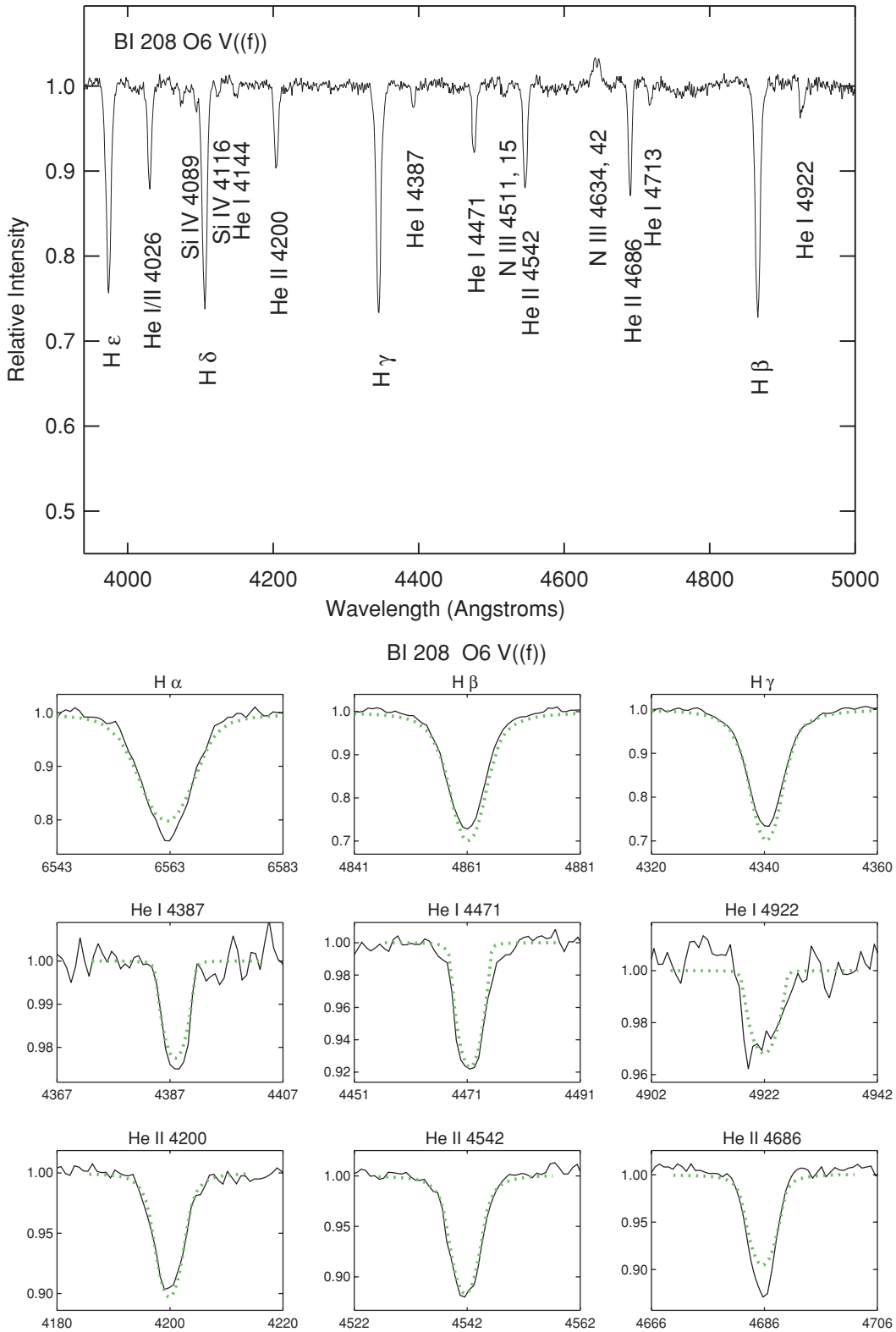

Figure 26. BI 208. The upper figure shows a section of the blue spectrum of this star, with the prominent lines identified. The lower figure shows the fits (dotted) for the principal diagnostic lines.

(A color version of this figure is available in the online journal.)

denote such stars in red. It is clear from the figure that this distinction is not really correct. In part, this is clarified by the addition of the new data here. There are stars of relatively lower mass with cooler temperatures which clearly show such an effect. Furthermore, such stars are not invariably supergiants, as was originally suggested for the Galactic example by Herrero

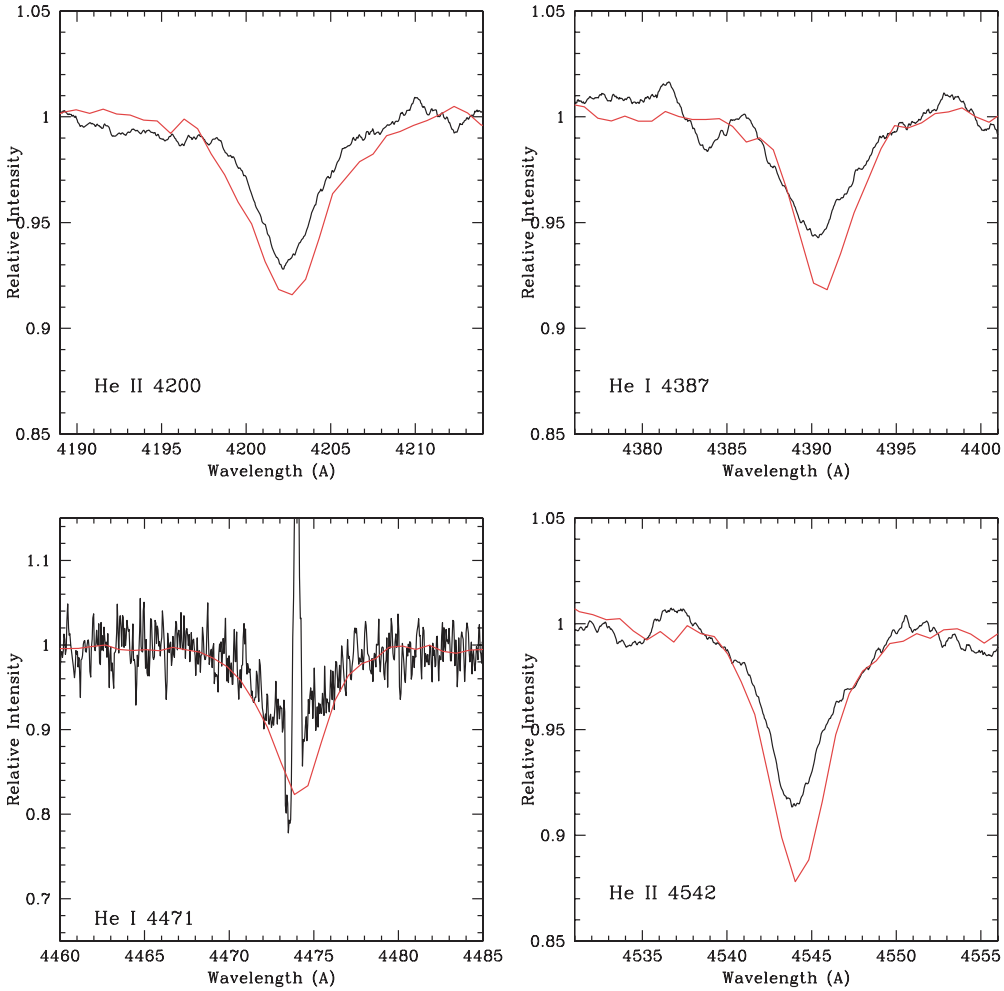

Figure 27. A comparison between some of the He I and He II lines from the Magellan data used by us (red) with the AAT data (black) used by Bouret et al. (2003) and Heap et al. (2006) for NGC 346−487. For all but the He I λ4471 data, the AAT data have been smoothed to match the resolution of the Magellan data. The AAT data were kindly provided by C. J. Evans (2005, private communication).

et al. (1992). We have searched for correlations between the size of the mass discrepancy with effective temperature and/or surface gravity, and find little connection. As we suggested in Paper II, it may be that in a few cases the answer is that a star has been affected by binary evolution, that is, LH 64−16, the giant shown at the top of the LMC plot. While the overall agreement in Figure 29 is encouraging, the figure shows that some improvement is still needed in either the atmosphere, the evolutionary models, or both. We note that we have used the older, nonrotating evolutionary models of Charbonnel et al. (1993) and Schaerer et al. (1993) in determining the evolutionary masses, but the use of the newer, rotating models, such as Meynet & Maeder (2005) (for which we do not have isochrones readily available) would exacerbate the differences rather than reduce them, as argued in Paper II.

5. SUMMARY AND FUTURE WORK

We have analyzed the spectra of 26 O and early B stars in the Magellanic Clouds, obtaining satisfactory fits to 18 stars. The effective temperatures we derive are in accord with the effective temperature scale we presented in Paper II. We emphasize that the "Of" indicators (N III λ4634, 42 and He II λ4686 emission) do not track the luminosity of the star in precisely the same manner as at Galactic metallicities, as the causes of the emission are different. With our very high S/N data, we are able to detect the weak He I λ4471 line in some of the earliest spectral types, providing strong constraints on the effective temperatures and other physical properties of these stars. We do find some significant differences with the work of others: the automatic FASTWIND fitting procedure of Mokiem et al. (2006, 2007) results in effective temperatures that are hotter than ours by 1100 K in the median, which is significant given that our estimated error is 500–1000 K. More interesting is the fact that Mokiem et al. (2006, 2007) found "best-fit" answers for stars for which we deemed no fit to be satisfactory. On average, the TLUSTY results of Bouret et al. (2003) and Heap et al. (2006) are 1000 K cooler than ours, although we note a problem with some of their data due to moonlight continuum contamination. There is still evidence of a discrepancy between the masses derived by spectroscopic analysis and those derived from the evolutionary tracks, in the sense that some stars have a significantly lower spectroscopic mass. The problem does not seem to be correlated with a single parameter (such as effective temperature), but is present for some stars and not for others.

In Paper II, we argued that the results from the literature suggest that there may be differences dependent upon what

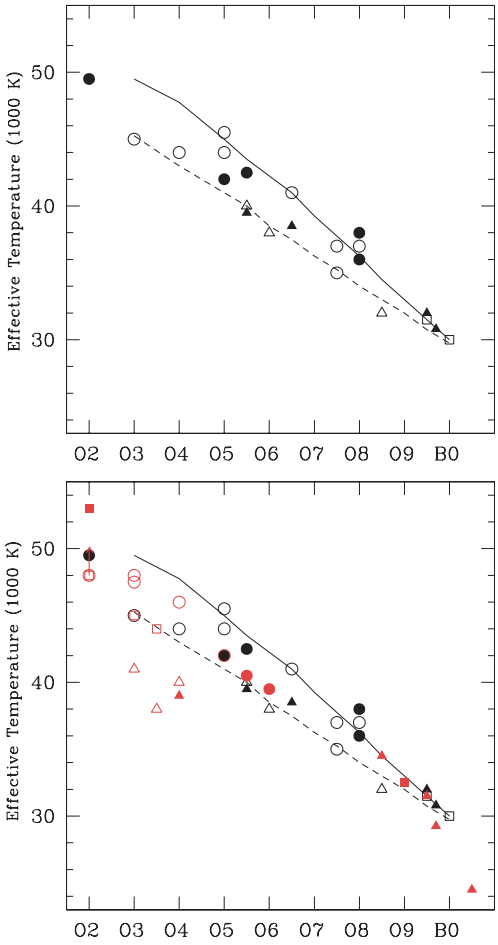

Figure 28. Effective temperature as a function of spectral type. Upper panel: the data for the SMC stars are shown here, with filled symbols representing the new data from this paper and open symbols representing the data from Papers I and II. Circles are dwarfs, boxes are giants, and triangles are supergiants. The solid line shows the Paper II calibration for SMC dwarfs and giants (corresponding to the circles and squares) and the dashed line that for supergiants (i.e., corresponding to triangles). Lower panel: same as for the top, but now with the LMC data added in red.

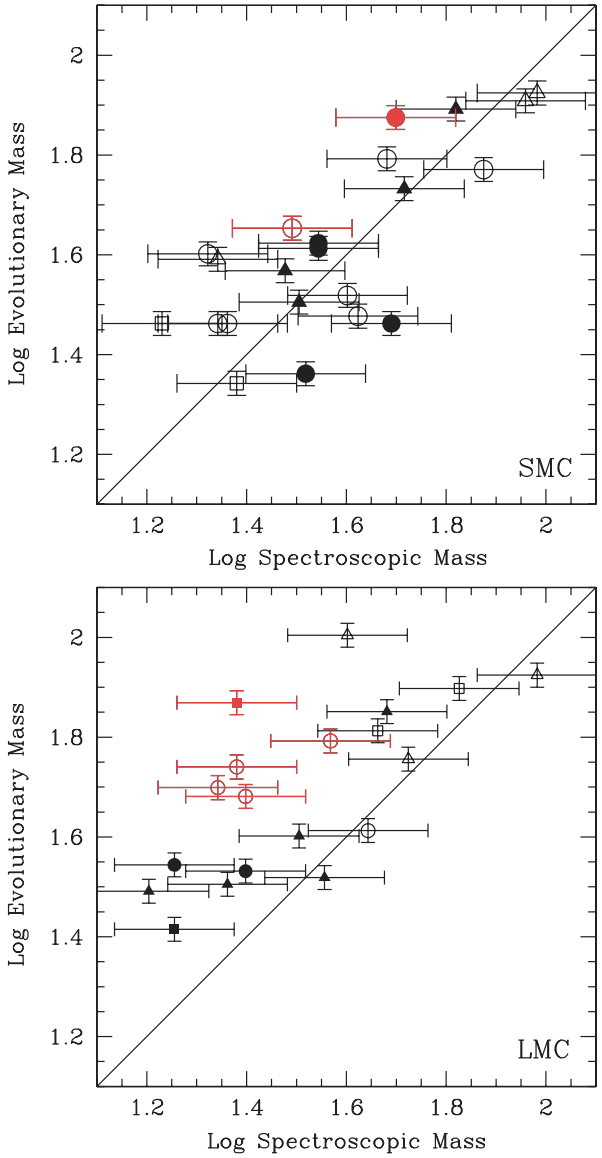

Figure 29. The mass discrepancy for our sample. Filled symbols denote the data new to this paper. Circles represent dwarfs, squares represent giants, and triangles represent supergiants. We have indicated in red the stars for which $T_{\rm eff}$ is greater than 45,000 K.

wavelength region is analyzed and even possibly what programs are used. The trouble with such comparisons in the past is that they have been based on samples with little or no overlap of individual stars. We plan to now analyze the UV spectra of the same stars analyzed in Papers I, II, and the present work to see how fits to the UV data compare with our FASTWIND optical results. In addition, we will analyze the same optical spectra by other means (e.g., CMFGEN; Hillier et al. 2003).

It is a pleasure to acknowledge the support of the Las Campanas Observatory in obtaining the optical spectra. Support for programs *HST* GO-9412, GO-9795, and AR-11270 was provided by NASA through grants from the Space Telescope Science Institute, which is operated by the Association of Universities for Research in Astronomy, Inc., under NASA contract NAS 5-26555. A.M.Z.'s work was supported through a National Science Foundation REU grant, AST-0453611. We are grateful to C. Evans for clarifying several issues for us in the past studies of some of the stars discussed here, as well as comments on an early draft. An anonymous referee made many useful suggestions which improved the paper.

REFERENCES

Asplund, M. 2003, in ASP Conf. Ser. 304, SNO in the Universe, ed. C. Harbonnel, D. Schaerer, & G. Meynet (San Francisco, CA: ASP), 275

Azzopardi, M., & Vigneau, J. 1975, A&AS, 22, 285

Bianchi, L., & Garcia, M. 2002, ApJ, 581, 610

Bouret, J.-C., Lanz, T., Hillier, D. J., Heap, S. R., Hubeny, I., Lennon, D. J., Smith, L. J., & Evans, C. J. 2003, ApJ, 95, 1182

Brunet, J. P., Imbert, M., Martin, N., Mianes, P., Prevot, L., Rebeirot, E., & Rousseau, J. 1975, A&AS, 21, 109

Buscombe, W., & Foster, B. E. 1995, MK Spectral Classifications (Evanston: Northwestern Univ.)

Charbonnel, C., Meynet, G., Maeder, A., Schaller, G., & Schaerer, D. 1993, A&AS, 101, 415

Conti, P. S. 1988, in O Stars and Wolf-Rayet Stars, ed. P. S. Conti & A. B. Underhill (NASA SP-497) (Washington, DC: NASA), 7

Conti, P. S., Garmany, C. D., de Loore, C., & Vanbeveren, D. 1983, ApJ, 274, 302

Crampton, D. C. 1979, ApJ, 230, 717

Crampton, D. C., & Greasley, J. 1982, PASP, 94, 31
Crowther, P. A., Hillier, D. J., Evans, C. J., Fullerton, A. W., De Marco, O., & Willis, A. J. 2002, ApJ, 579, 774
de Koter 2008, in IAU Symp. 250, Massive Stars as Cosmic Engines, ed. F. Bresolin, P. A. Crowther, & J. Puls (Cambridge: Cambridge Univ. Press), 39
Evans, C. J., Lennon, D. J., Trundle, C., Heap, S. R., & Lindler, D. J. 2004, ApJ, 607, 451
Garmany, C. D., Conti, P. S., & Massey, P. 1980, AJ, 242, 1063
Garmany, C. D., Conti, P. S., & Massey, P. 1987, AJ, 93, 1070
Groenewegen, M. A. T., Lamers, H. J. G. L. M., & Pauldrach, A. W. A. 1989, A&A, 221, 78
Hamann, W.-R., Oskinova, L. M., & Feldmeier, A. 2008, Proc. International Workshop on Clumping in Hot-Star Winds (Potsdam: Universitätsverlag Potsdam)
Heap, S. R., Lanz, T., & Hubeny, I. 2006, ApJ, 638, 409
Herrero, A. 2003, in IAU Symp. 212, A Massive Star Odyssey, from Main Sequence to Supernova, ed. K. A. van der Hucht, A. Herrero, & C. Esteban (San Francisco, CA: ASP), 3
Herrero, A., Kudritzki, R. P., Vilchez, J. M., Kunze, D., Butler, K, & Haser, S. 1992, A&A, 261, 209
Hillier, D. J., Lanz, T., Heap, S. R., Hubeny, I., Smith, L. J., Evans, C. J., Lennon, D. J., & Bouret, J. C. 2003, ApJ, 388, 1039
Kudritzki, R. P., & Puls, J. 2000, ARA&A, 38, 613
Lucke, P. B. 1973, PhD thesis, Univ. Washington
Martins, F., & Plez, B. 2006, A&A, 457, 637
Martins, F., Schaerer, D., & Hillier, D. J. 2002, A&A, 382, 999
Martins, F., Schaerer, D., & Hillier, D. J. 2005, A&A, 436, 1049
Massey, P. 1998a, in ASP Conf. Ser. 142, The Stellar Initial Mass Function, 38th Herstmonceux Conference, ed. G. Gilmore & D. Howell (San Francisco, CA: ASP), 17
Massey, P. 1998b, in Stellar Astrophysics for the Local Group, ed. A. Aparicio, A. Herrero, & F. Sanchez (Cambridge: Cambridge Univ. Press), 95
Massey, P. 2002, ApJS, 141, 81
Massey, P., Bresolin, F., Kudritzki, R. P., Puls, J., & Pauldrach, A. W. A. 2004, ApJ, 608, 1001, (Paper I)
Massey, P., & Conti, P. S. 1977, ApJ, 218, 431
Massey, P., Parker, J. W., & Garmany, C. D. 1989, AJ, 98, 1305
Massey, P., Puls, J., Pauldrach, A. W. A., Bresolin, F., Kudritzki, R. P., & Simon, T. 2005, ApJ, 627, 477 (Paper II)
Massey, P., Valdes, F., & Barnes, J. 1992, A User's Guide to Reducing Slit Spectra with IRAF (Tucson, AZ: NOAO), http://www.iraf.net/irafdocs/spect/
Massey, P., Waterhouse, E., & DeGioia-Eastwood, K. 2000, AJ, 119, 2214
Meynet, G., & Maeder, A. 2005, A&A, 429, 581
Mihalas, D., Hummer, D. G., & Conti, P. S. 1972, ApJ, 175, L99
Mokiem, M. R., de Koter, A., Puls, J., Herrero, A., Najarro, F., & Villamariz, M. R. 2005, A&A, 447, 711
Mokiem, M. R., et al. 2006, A&A, 456, 1131
Mokiem, M. R., et al. 2007, A&A, 465, 1003
Najarro, F., Hillier, D. J., Puls, J., Lanz, T., & Martins, F. 2006, A&A, 456, 659
Niemela, V. S., Marraco, H. G., & Cabanne, M. L. 1986, PASP, 98, 1133
Press, W. H., Teukolsky, S. A., Vetterling, W. T., & Flannery, B. P. 1992, Numerical Recipes in Fortran (Cambridge: Cambridge Univ. Press), 651
Prinja, R. K., & Crowther, P. A. 1998, MNRAS, 300, 828
Puls, J., Urbaneja, M. A., Venero, R., Repolust, T., Springman, U., Jokuthy, A., & Mokiem, M. R. 2005, A&A, 435, 669
Puls, et al. 1996, A&A, 305, 171
Repolust, T., Puls, J., & Herrero, A. 2004, A&A, 415, 349
Russell, S. C., & Dopita, M. A. 1990, ApJS, 74, 93
Sanduleak, N. 1970, Contribution Cerro Tololo Inter-American Observatory, No. 89
Santolaya-Rey, A. E., Puls, J., & Herrero, A. 1997, A&A, 323, 488
Schaerer, D., Meynet, G., Maeder, A., & Schaller, G. 1993, A&AS, 98, 523
van den Bergh, S. 2000, The Galaxies of the Local Group (Cambridge: Cambridge Univ. Press)
Voels, S. A., Bohannan, B., & Abbott, D. C. 1989, ApJ, 340, 1073
Walborn, N. R. 1973, ApJ, 186, 611
Walborn, N. R. 1977, ApJ, 215, 53
Walborn, N. R., & Fitzpatrick, E. L. 1990, PASP, 379
Walborn, N. R., Lennon, D. J., Haser, S. M., Kudritzki, R. P., & Voels, S. A. 1995, PASP, 107, 104
Walborn, N. R., Lennon, D. J., Heap, S. R., Linder, D. J., Smith, L. J., Evans, C. J., & Parker, J. W. 2000, PASP, 112, 1243
Walborn, N. R., Morrell, N. I., Howarth, I. D., Crowther, P. A., Lennon, D. J., Massey, P., & Arias, J. I. 2004, AJ, 608, 1028
Walborn, N. R., et al. 2002, AJ, 123, 2754
Westerlund, B. E. 1997, The Magellanic Clouds (Cambridge: Cambridge Univ. Press)